isvr Institute of Sound and Vibration Research

Numerical Investigation into the Radiation of Sound from Railway Wheels

T. Bruneteau, C.J.C. Jones and D.J. Thompson

ISVR Technical Memorandum 841

August 1999

University of Southampton

SCIENTIFIC PUBLICATIONS BY THE ISVR

Technical Reports are published to promote timely dissemination of research results by ISVR personnel. This medium permits more detailed presentation than is usually acceptable for scientific journals. Responsibility for both the content and any opinions expressed rests entirely with the author(s).

Technical Memoranda are produced to enable the early or preliminary release of information by ISVR personnel where such release is deemed to the appropriate. Information contained in these memoranda may be incomplete, or form part of a continuing programme; this should be borne in mind when using or quoting from these documents.

Contract Reports are produced to record the results of scientific work carried out for sponsors, under contract. The ISVR treats these reports as confidential to sponsors and does not make them available for general circulation. Individual sponsors may, however, authorize subsequent release of the material.

UNIVERSITY OF SOUTHAMPTON

INSTITUTE OF SOUND AND VIBRATION RESEARCH

DYNAMICS GROUP

Numerical Investigation into the Radiation of Sound from Railway Wheels

by

T. Bruneteau, C.J.C. Jones and D.J. Thompson

ISVR Technical Memorandum No. 841

August 1999

Authorized for issue by
Dr M.J. Brennan
Group Chairman

ABSTRACT

The sound radiated by a railway wheel is investigated using boundary element calculations. The axi-harmonic formulation is used in which the wheel is defined by a two-dimensional mesh of its cross-section and the motion is decomposed into harmonics of different numbers of nodal diameters. The radiation ratios of the wheel, vibrating in its various normal modes, are calculated for a range of frequencies. The effects of wheel radius, web thickness and tyre depth are also investigated. Finally semi-analytical formulae are derived that allow the radiation ratios to be approximated closely. These are more convenient than boundary element calculations for calculating the rolling noise from a wheel.

CONTENTS

1. INTRODUCTION

Rolling noise is the most important source of environmental noise from railways at conventional speeds. It is radiated by vibrations of the wheels, rails, and sleepers excited by the roughness of the wheel and rail running surfaces. Since the 1970s theoretical models have been developed to predict the generation of rolling noise. This has culminated in the development of the TWINS program [1].

Within TWINS, the calculation of the sound radiation from the wheel is based on a series of simple formulae for the radiation ratio that were derived from comparison with Boundary Element calculations [2]. At the time of these original calculations (1991) the Boundary Element software used (Sysnoise) could not perform an axisymmetric calculation with diametral nodes, so the dependence on the number of such nodes was obtained by comparison with Rayleigh Integral calculations.

A recent study [3] has led to the development of a specially made boundary element program with an axisymmetric formulation in which the structure is modelled in two dimensions but the vibration may be decomposed into Fourier components of different numbers of nodal diameters. This was used to update the formulae in TWINS [4]. However, some numerical instabilities were found that could not be resolved and it was desirable to repeat these calculations using proprietary software.

Recent versions of Sysnoise [5] have implemented also such an axisymmetric formulation. The purpose of the current study is therefore to use the latest version of Sysnoise to investigate more thoroughly the dependence of the wheel radiation ratio on the number of nodal diameters as well as the wheel dimensions. Moreover, parameters variations are included to ensure that the dependence on wheel radius, tyre depth and web thickness is properly accounted for.

2. WHEEL RADIATION IN TWINS

2.1 Prediction of vibration

The prediction of the wheel vibration in TWINS is made in terms of modal superposition. The modes of a wheel, like those of a disk, are either principally axial or radial. These various modes are categorised by the number of nodal diameters (n = 0, 1, 2, 3, ...) and (for axial modes) the number of nodal circles (m = 0,1,2,...); see Figure 2.1. The 0-nodal-circle modes, with a maximum amplitude at the tread in the axial direction, are usually found to be excited in curve squeal, but are much less important in rolling noise. On the other hand, both radial and 1-nodal-circle modes are important in rolling noise. A coupling effect occurs due to the asymmetry of the wheel web so that both sets of modes contain a significant amount of axial motion and radial motion, which is not the case for a flat disc.

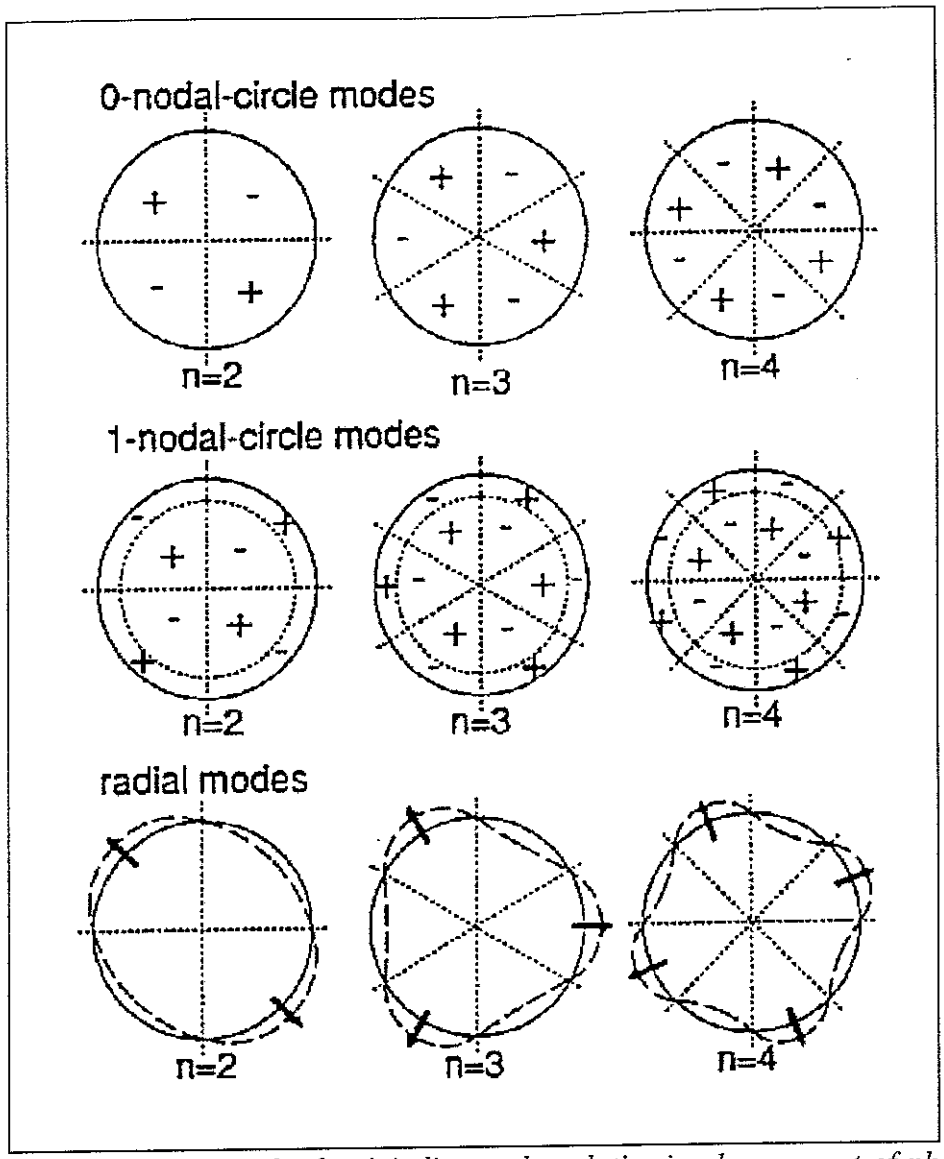

Figure 2.1: Modeshapes of a wheel. +/- indicates the relative in-phase or out-of-phase motion in each area.

In a TWINS prediction, the wheel response during rolling is calculated in terms of the vibration spectra at a series of positions. Each spectrum represents the response at this position, averaged around the wheel. Usually 4-6 axial positions are used, one of which is located on the tyre (see Appendix A for the details of a wheel) and the rest on the web at various radii. The vibration of the tyre is expressed as axial, radial and torsional components, assuming that the tyre does not deform significantly in cross-section. All of these spectra are calculated taking account of wheel rotation. They are also decomposed into components associated with modes of different numbers of nodal diameters.

2.2 Prediction of sound radiation

The wheel radiation is calculated in TWINS using 1/3 octave vibration data predicted by the wheel response module. The sound power radiated by a wheel is calculated in the TWINS software in terms of three components of vibration, which are assumed independent:

- axial component of vibration of the wheel web and tyre (subscript a)
- radial vibration of the wheel tyre (subscript r)
- rotational (torsional) vibration of the wheel tyre (subscript t)

For each of these vibrational components a separate radiation ratio is calculated using semi-analytical formulae which have been derived from boundary element calculations [2]. These radiation ratios depend strongly at low frequencies on the circumferential order n.

The total sound power radiated by the wheel at each frequency is calculated using (see [1,2]):

$$W^W = \rho c \sum_n \left(\sigma_a(n) \sum_j \left(S_{aj} \overline{\tilde{v}_{ajn}^2} \right) + \sigma_r(n) S_r \overline{\tilde{v}_{rn}^2} + \sigma_t(n) S_t \overline{\tilde{v}_{tn}^2} \right) \qquad (2.1)$$

where ρ is the density of air,
c is the speed of sound in air,
S_r is the surface area associated with radial vibration (etc),
$\overline{\tilde{v}_{rn}^2}$ is the spatially averaged (around the circumference), mean square vibrational velocity for circumferential order n in the radial direction (etc),
$\sigma_r(n)$ is the radiation ratio for circumferential order n for radial vibration (etc)

From equation (2.1) it can be seen that at each frequency and each circumferential order n, a single velocity is used for radial and rotational vibration. For axial vibration the velocities at various positions (j) are used. Each has its own associated area, S_{aj}, but a single radiation ratio is used for all of the axial vibration. The radiation ratios used for these three components are presented below.

2.3 Radiation ratios

Within the current version (v2.4) of TWINS, the radiation ratio applying to axial vibration of circumferential order n is given by

$$\sigma_a(n) = \frac{1}{1 + \left(f_{ca}(n) / f \right)^{2n+4}} \text{ where } f_{ca}(n) = \frac{c}{2\pi R} \sqrt{(n+1)(n+4)} \qquad (2.2, 2.3)$$

where R is the wheel radius. For radial vibration of circumferential order n,

$$\sigma_r(n) = \frac{1}{1 + \left(f_{cr} / f \right)^{2n+2}} \text{ where } f_{cr} = \frac{c}{\sqrt{2}\,\pi w} \qquad (2.4, 2.5)$$

where w is the tread width. The critical frequency f_{cr} in this case was revised in ref. [4] (previously it was dependent on n). The radiation ratio applying to torsional vibration of the tyre of circumferential order n was revised in ref. [4] and is given by

$$\sigma_t(n) = \frac{1}{1 + \left(f_{ct}(n) / f \right)^4} \text{ where } f_{ct}(n) = \frac{2c}{\pi w} \sqrt{(n+1)(n+4)} \qquad (2.6, 2.7)$$

In fact the torsional motion of the tyre does not contribute significantly to the souind radiation from a wheel, and will not be considered further in this report.

3. ANALYSIS METHOD

3.1 Overview

In the current study, the radiation ratio for various wheel geometries has been studied. The method used consists of the following steps.

1. The modes of vibration of the wheel in question are calculated using an axisymmetric finite element model. For this ANSYS [6] is used.
2. For each mode of vibration, an input data file for the boundary element calculation is produced incorporating the normal vibration on the surface.
3. The sound radiation is calculated for each mode shape for a wide range of frequencies using the boundary element method. For this SYSNOISE [5] is used.
4. The radiation ratio results as a function of frequency are exported to Matlab for further processing and comparison with the formulae given above.

Descriptions of the finite element and boundary element methods are given in Appendices B and C. In the following sections particular aspects of the implementation for this study are discussed.

3.2 Wheels studied

The study is based initially on a 920 mm diameter (0.46 m radius) standard freight wheel, also considered in [4]. This is shown in Figure 3.1.

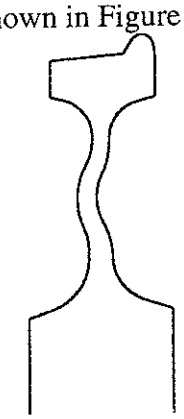

Figure 3.1. Section of the reference wheel.

In addition some variants are considered, listed below and shown in Figure 3.2:

- Straight webbed wheel, radius 0.38 m,
- Straight webbed wheel, radius 0.42 m,
- Straight webbed wheel, radius 0.46 m,
- Straight webbed wheel, radius 0.50 m,
- Straight webbed wheel, radius 0.42 m, wide web (76 mm instead of 25 mm)
- Straight webbed wheel, radius 0.42 m, full web (127 mm instead of 25 mm)
- Straight webbed wheel, radius 0.42 m, thick tyre (c. 120 mm instead of 60 mm),
- Straight webbed wheel, radius 0.42 m, thin tyre (c. 30 mm instead of 60 mm).

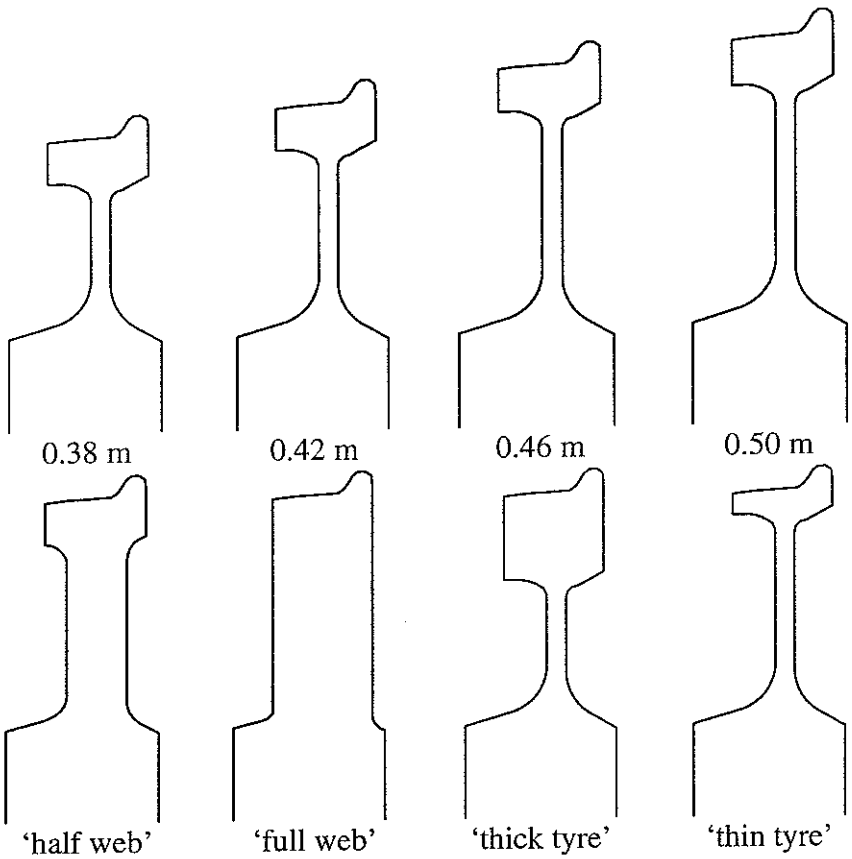

Figure 3.2: Sections of the 'straight webbed' wheels.

3.3 Finite element calculations

The finite element calculations (Appendix B) were carried out using the ANSYS package. For the present work the mode shapes were required in order to specify suitable boundary conditions in terms of the normal velocity on the surface for the sound radiation calculations. A modal analysis for each wheel was therefore carried out.

The radial cross-section of the wheel was entered using co-ordinates taken from the wheel drawing. The cross-section was meshed using the 8-noded element type PLANE 83 which is provided for axi-harmonic analyses. The axle is not included in the finite element model. Instead the displacements at the inside cylindrical surface of the hub are constrained. The use of such a model including the wheel has been found previously to reproduce the mode shapes of the wheel accurately enough for the TWINS model even in the case of the 1 nodal diameter modes which include bending of the axle. Moreover, in the present work, the modal frequencies are not required at all.

Initially, the mesh size was set small enough to make sure that a wavelength in air contains at least 6 elements at the highest frequency in the range of interest (6000 Hz).

The solution for the mode shapes was repeated for each successive number of nodal diameters from zero to seven. This number of harmonics was defined in the 'other' option in ANSYS. The soultion procedure based on a reduced number of degrees of freedom was chosen, using 100 automatically chosen 'master' degrees of freedom.

To write the results into the results file (filename *jobname*.rst) it is necessary to leave the solution menu, finish the analysis, and return to the solution part, so the command 'expansion pass' can be executed. Solving the problem at this stage expands the reduced solution to the full DOF set, and also writes the mode shapes into the results file.

The mode shapes were reviewed using the ANSYS general postprocessor so that each mode written to results file was identified as one of:

- zero-nodal circle axial mode
- one-nodal circle axial mode
- two-nodal circle axial mode
- radial mode

This results file is the one that SYSNOISE is able to use to pick up the mode-shape displacements to apply as velocity boundary conditions.

An additional set of boundary conditions was required, consisting of pure radial motion of the tyre part of the wheel. For this, another results file was created in ANSYS. To do so, every degree of freedom along the web was constrained, as were the y and z ones on the tyre. However, these being significant constraints, it was necessary to modify the stiffness of the structure to ensure results were obtained in the frequency range. Lowering the Young's modulus from 2.1×10^{11} to 5×10^{10} N/m^2 provided results in the range of interest. This modification to the structure did not affect later calculations. Indeed, the boundary displacements are used across the whole range of frequency whatever the natural frequency of the motion considered.

3.4 Boundary element calculations

The SYSNOISE package was used for the radiation calculations (Appendix C). The Indirect Boundary Element Method was chosen since this option has the more satisfactory method of dealing with numerical difficulties for the external radiation problem and also since it is the only option available in Sysnoise for solutions for axi-harmonic boundary conditions on axisymmetric structures.

The mesh used by the indirect boundary element method of SYSNOISE is not the same as the one used in the ANSYS calculation. This one only defines the surface of the wheel.

It is necessary, when performing the axi-harmonic analyses of the wheel models, to ensure that SYSNOISE is able to access sufficient computer memory space. It was found sufficient to specify the option '-m12' on the command line when running SYSNOISE (this allocates 12×4 MB of memory space).

The 2D shape has been meshed by ANSYS and imported in SYSNOISE as a cdb file. It is created by ANSYS under the 'archive model' option in the preprocessor. This shape has to generate a closed surface. The consistency of the normal vectors has to be checked, *i.e.* all of them have to point outwards. Boundary elements where the normal vector was defined in the wrong direction by ANSYS were therefore reversed.

The structural results from the *jobname*.rst file created by ANSYS are used to provide the boundary conditions to SYSNOISE. The set of elements from the BEM mesh has to fit the location of the boundary conditions in the structural mesh.

The wheel is studied in its different modes. The displacements recorded in the results file are automatically converted into normal velocities, v, (Neumann boundary condition) by the expression:

$$v = i.\omega.\vec{u}.\vec{n} \tag{3.1}$$

where $\vec{u}$ is the nodal displacement vector and $\vec{n}$, the normal vector.

Once the boundary conditions have been defined, the mesh can be converted into a 'pseudo 3D' mesh with the 'axisymmetry' command. This leads to a dialogue box requesting a 'refinement number', r, and the maximum harmonic number, M, to be specified. The number r will define the number of sectors used (2^r) to generate an approximation to the axisymmetric surface. This surface is used as the generator for the Fourier series approximation of the boundary conditions passed from the finite element program, which may be generally non-axisymmetric as far as SYSNOISE is concerned. The number M defines the highest order term of the series expansion:

$$v(x,y,\theta) = \sum_{n=-M}^{M} f_n(x,y).e^{jn\theta} \tag{3.2}$$

Note that the $n = 0$ term corresponds to axisymmetric boundary conditions.

The present analysis presents a distribution of velocity from the ANSYS-generated modes which corresponds to only a single term at a time in the above expansion.

To minimise the memory space used, it is necessary to use as small a refinement number, r, as possible. The axisymmetry refinement does not have influence on the calculations except that it limits the series to the number of harmonics $2^{(r-1)}$. It is essential therefore that r be set large enough to generate the (single) term of the series required to reproduce the axi-harmonic variation specified for the mode shape within ANSYS.

The boundary conditions being defined before the axisymmetry definition, they are perfectly defined as being axi-harmonics. It has been checked that, with boundary conditions set at a selected harmonic, null results were provided at all other terms of the Fourier expansion. The global result was therefore the same as the result for the n^{th} term. However, it was chosen to select n explicitly in the 'frequency response' part of the SYSNOISE command to prevent from any mistake in the selection of the refinement r.

Since the procedure used in SYSNOISE is somewhat complicated, an example journal file listing is given in Appendix D. This represents the procedure for calculation settled upon after the investigations described in Section 3.5.

3.5 Ensuring accuracy of the solution procedure

It was found that the calculation of radiation ratios using the surface solution, which is carried out automatically at solution time in SYSNOISE, was not completely stable and at high frequencies the variation of the radiation ratio with frequency that was obtained was not smooth having occasional values much higher that 1 and, in some cases, negative values. The SYSNOISE vendors, LMS, explain that these results arise from cancellations of values in the integration of the sound power at the sharp corners of the structural model. To solve this problem, a spherical field point mesh surface, some distance away from the radiating surface, was used and the intensity passing through that surface was integrated to find the radiated sound power and hence the radiation ratio.

However, this introduces possible inaccuracy due to the required refinement of the spherical surface mesh. The sphere is obtained by deformation of a cube, each face of which is subdivided into $N \times N$ elements. A low value of N gave an attenuated radiation ratio at high frequencies, where it is expected to converge towards unity. Some experimentation led to the conclusion that a generator number, $N = 60$ is adequate for the frequency range up to 6000 Hz.

For each mode shape of each wheel, calculations of the radiation ratio were performed for 100 logarithmically spaced frequency steps from 50 to 6000 Hz.

In order to obtain the most efficient method of simulation, results for several mesh refinements were compared. The structural mesh, the geometrical mesh, and the axisymmetric set up were changed. Eventually the best field point mesh has been defined to obtain accurate results in the frequency range chosen. These comparisons were made with the reference wheel in its 0-nodal-circle, 2-nodal-diameter mode.

3.5.1 Influence of the structural mesh refinement.

ANSYS gives the possibility to refine a mesh which already exists. The command 'Refinement 1' would create a mesh the elements of which are approximately half the size of the original ones. It has also been refined to a quarter of the size ('Refinement 3'). A calculation has been done for each case. The results are drawn in the following figure, presented with the difference between the finest mesh and the original mesh.

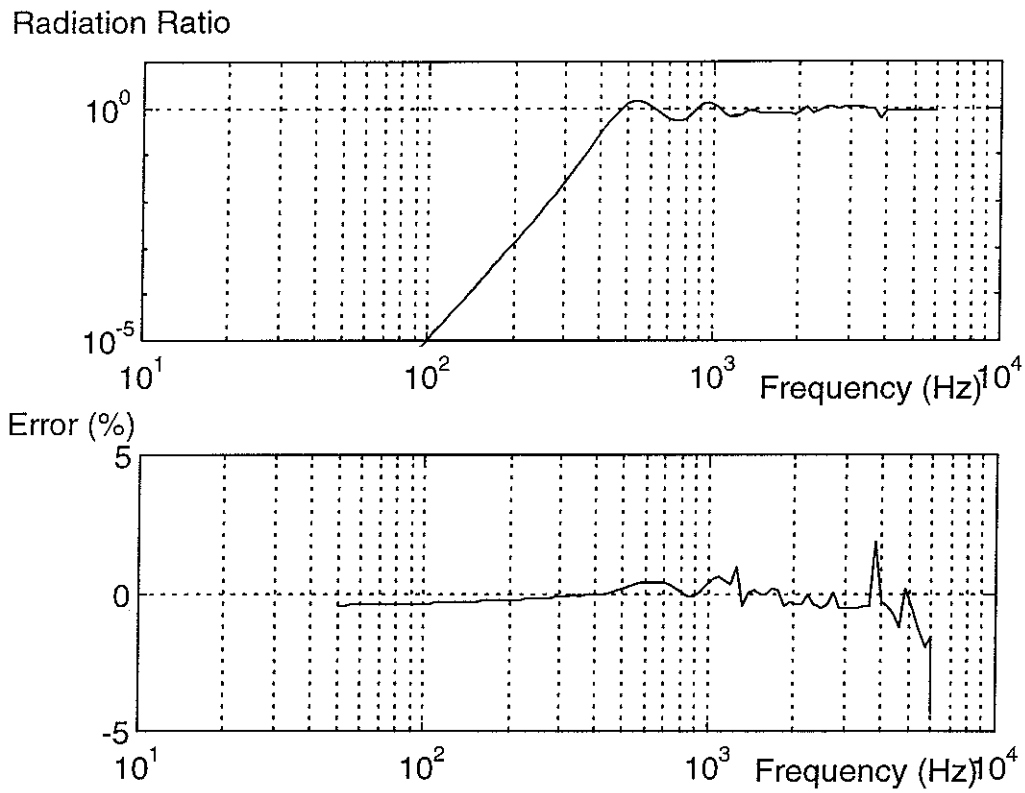

Figure 3.2. Error committed due to the degree of structural mesh refinement used (comparison of original mesh and mesh with one quarter of the element size).

The curves are very close, which is confirmed by the second graph, that shows a maximum error of less than 5%. The structural mesh is therefore sufficiently fine to ensure that it does not have much influence on the accuracy of the results.

3.5.2 Influence of the geometric mesh refinement.

The geometric boundary mesh was refined in ANSYS, creating mesh elements of 5 and 2 mm. The original mesh had elements about 10 mm long. The influence on the radiation ratio is given in the following figure.

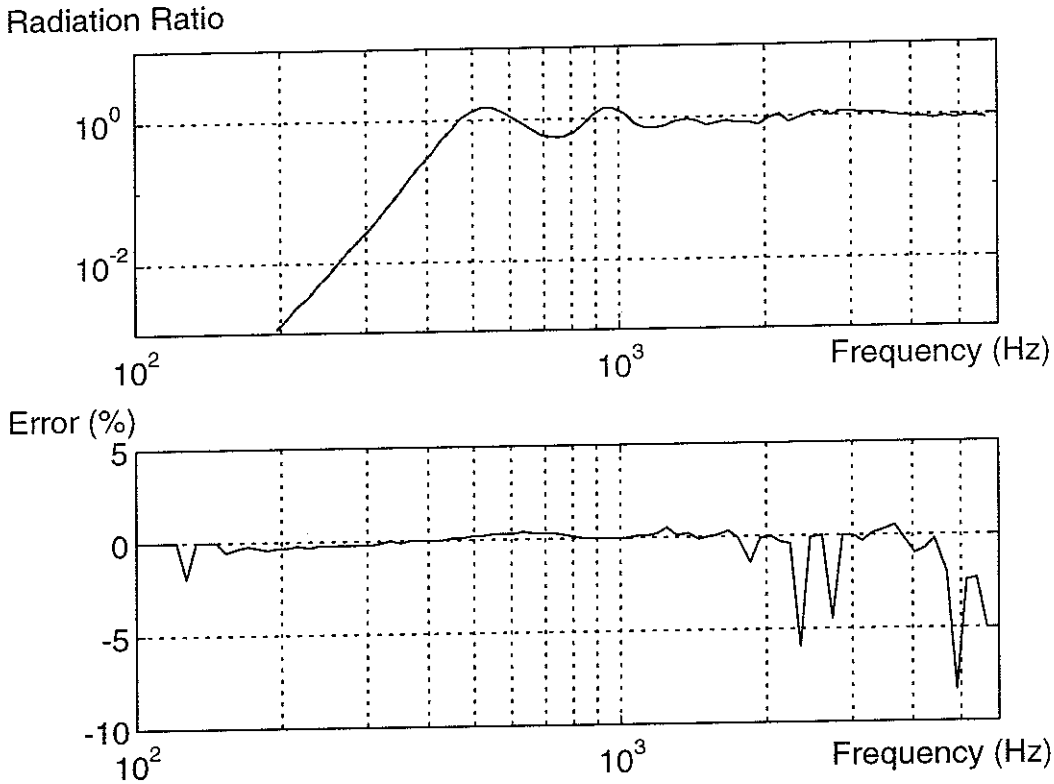

Figure 3.3. Error committed due to the degree of geometric mesh refinement used (Comparison of chosen mesh with 10 mm elements and mesh with 2 mm elements).

Here again, the results are rather close from one mesh to the other. The error does not exceed 8%.

3.5.3 Influence of the axisymmetric refinement.

The refinement number r in SYSNOISE is found to have no influence on the results as long as the refinement permits the study of the chosen harmonic. However, the calculations take far longer with a higher refinement number, so the smallest possible value should always be used.

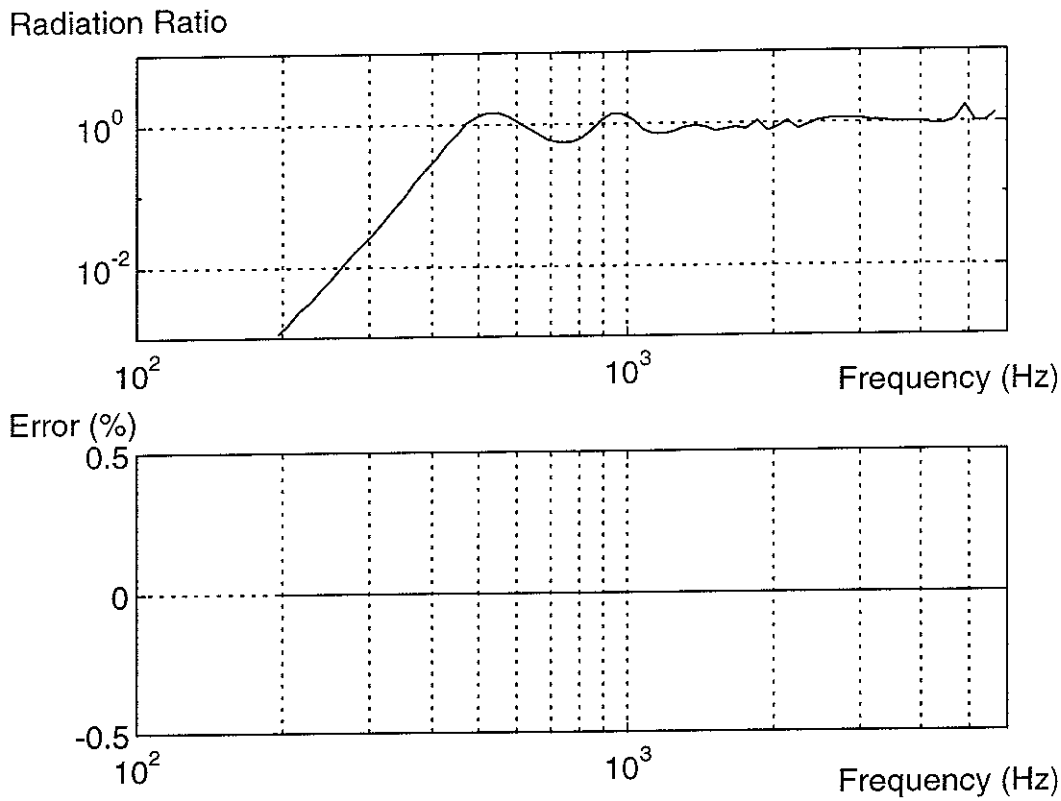

Figure 3.4. Error committed for the degree axisymmetric refinement used (comparison of calculations with r=2 and r=3).

3.5.4 Influence of the field point mesh refinement.

Initially, the results at high frequencies differed from those expected, as they sloped downwards above the critical frequency. The following figure shows the cause to be the field point mesh. As already mentioned above, the sphere is the deformation of a cube, the faces of which are divided into N × N elements. The different calculations of radiation ratios for N=6, N=10, N=60 and N=100 are displayed on the following graphs. Assuming that N=100 gives very accurate results, the error introduced using N=60 is also plotted.

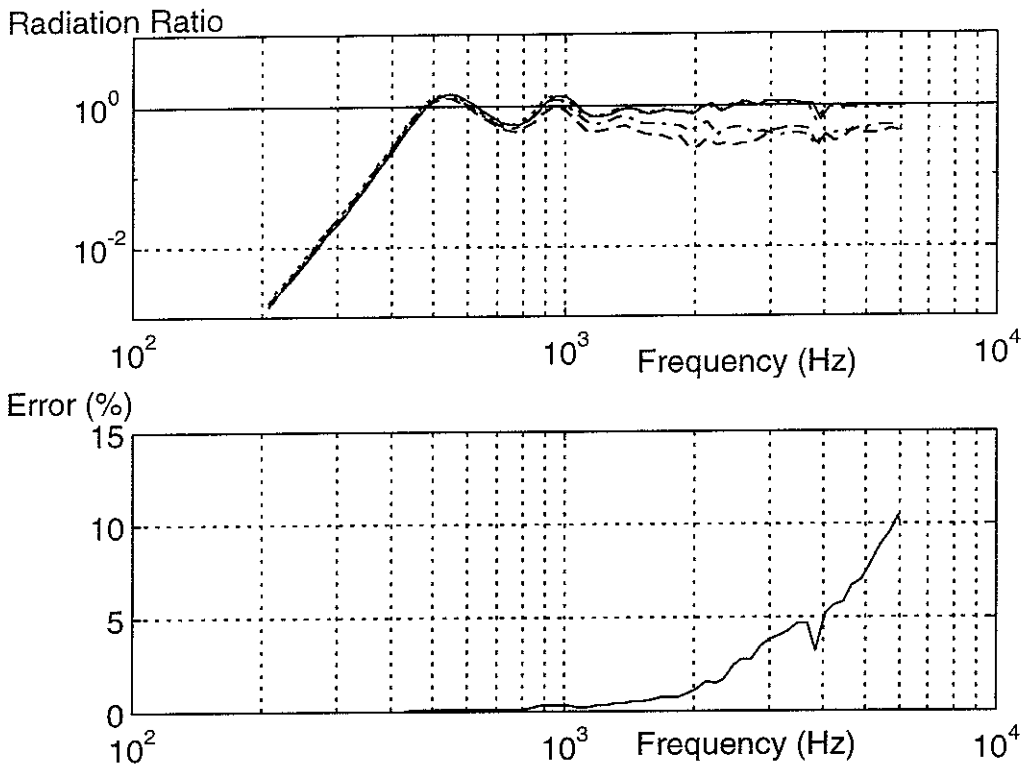

Figure 3.5. Error committed for the degree of field point mesh refinement used.
——, N=100; - - - - -, N=60; — -, N=10; — —, N=6.
Lower: difference between N=60 and N=100.

We see here that for 60 elements, the results in the frequency range chosen are acceptable; the errors stay under 10%, which is only reached at the very end of the frequency range.

3.6 Effects of mesh refinement

These investigations permitted to define the meshes used for the modelling. In the results presented in the remainder of the report, the given meshes are used for the structural calculations (elements of approximate length 1 cm) and the geometric calculations (approximate length: 1 cm). The axisymmetric refinement, r, is chosen high enough to permit the calculation at the harmonic selected, but otherwise, as small as possible. The table below shows the values used:

r	1	2	3	4
used for harmonics	0, 1	2	3, 4	5 to 8

Table 3.1. Values used for the axisymmetric refinement, r.

Last, the field point mesh refinement is set at N=60, as it provides reasonably accurate results.

4. RESULTS

4.1 Data treatment

The command 'Inquire Power' in SYSNOISE provides a text file with all the calculations processed during the session across the frequency range: Input Power[1], Mean Square Velocity, Output Active Power, Output Reactive Power, and Radiation Ratio along the surface, and the Output Active and Reactive Power across the field point mesh. The results of interest are the output active power across the field point mesh and the 'input power' which allow to calculate the radiation ratios.

For each wheel, results are given for the 0-nodal-circle axial modes, the 1-nodal-circle axial modes and the pure radial motion of the tyre. All the radiation ratios (for all the numbers of nodal diameters available) of each series are plotted on one graph.

Despite taking great care to achieve good accuracy in the mesh definition, the results show some unexpected behaviour, particularly at high frequency. At some specific frequencies the results differed greatly from adjacent frequencies, which is believed not to be a physical but a numerical phenomenon. In plotting the results, the worst of these discontinuities have been omitted.

The approximations of radiation ratios given in Section 2.3 are plotted within these graphs. However, the equations give the ratio versus the frequency with critical frequency as parameter. In this section, rather than use the critical frequencies given in Section 2, the curves have been fitted to the boundary element results. This is done by choosing to fit the value of the formula to the boundary element results at the radiation ratio $\sigma_0 = 0.01$. For this an interpolation between the closest values is used (see appendix E for an example of data treatment). This allows then to find the critical frequency in the approximate equation and thus, plot σ versus the frequency.

These plots are given in the next three sdections. For the axial modes these are followed by plots of $f_c \times R$ versus n, the number of nodal diameters, R being the radius of the wheel. For the radial motion $f_c \times w$ is plotted versus n, w being the thickness of the tread.

[1] In SYSNOISE terminology Input Power is $\rho c S \langle v^2 \rangle$.

4.2 Results for 0-nodal-circle axial modes

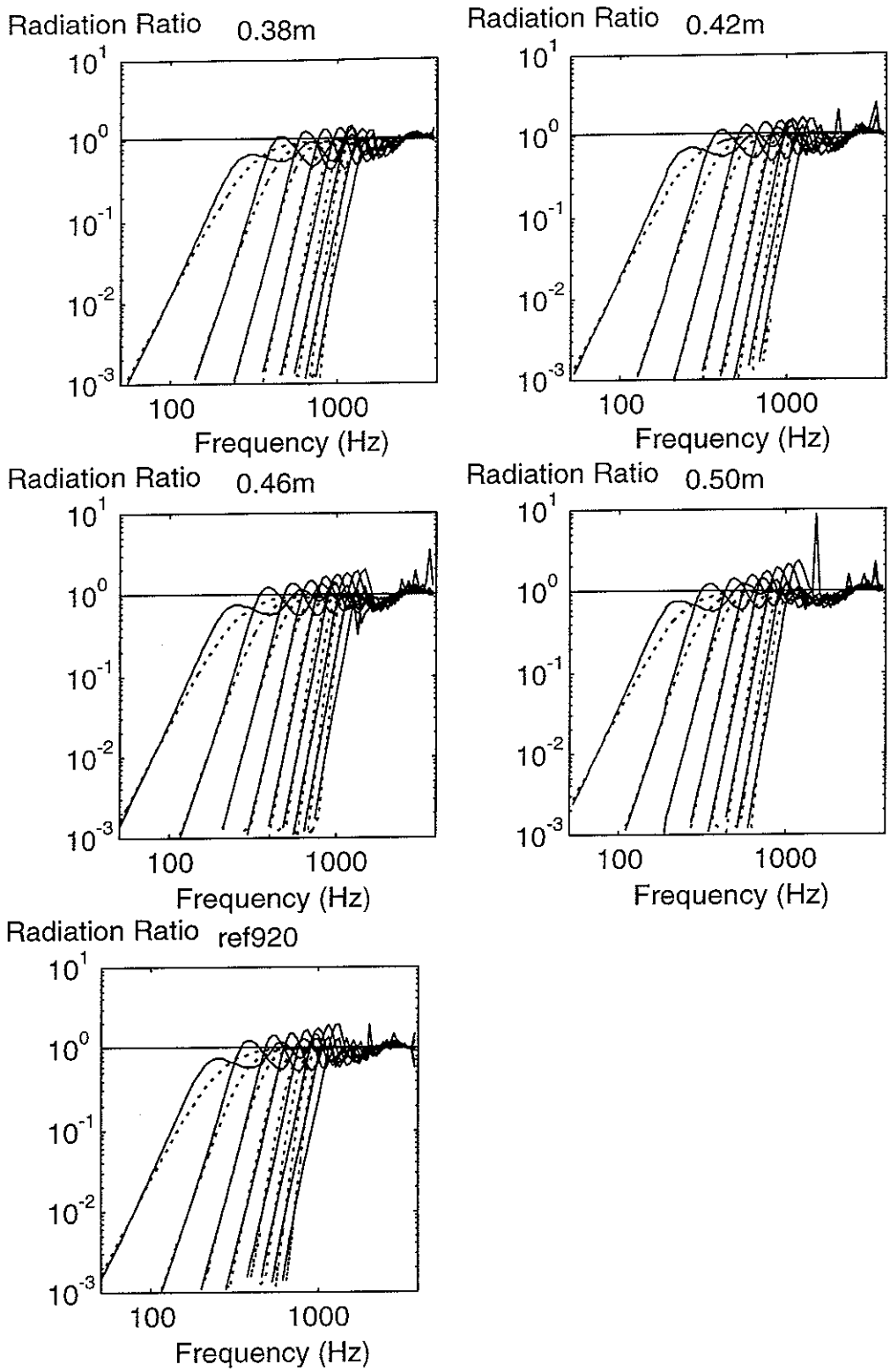

Figure 4.1. Results for 0-nodal-circle axial modes.
——, BE modelling results; - - -, approximation results.

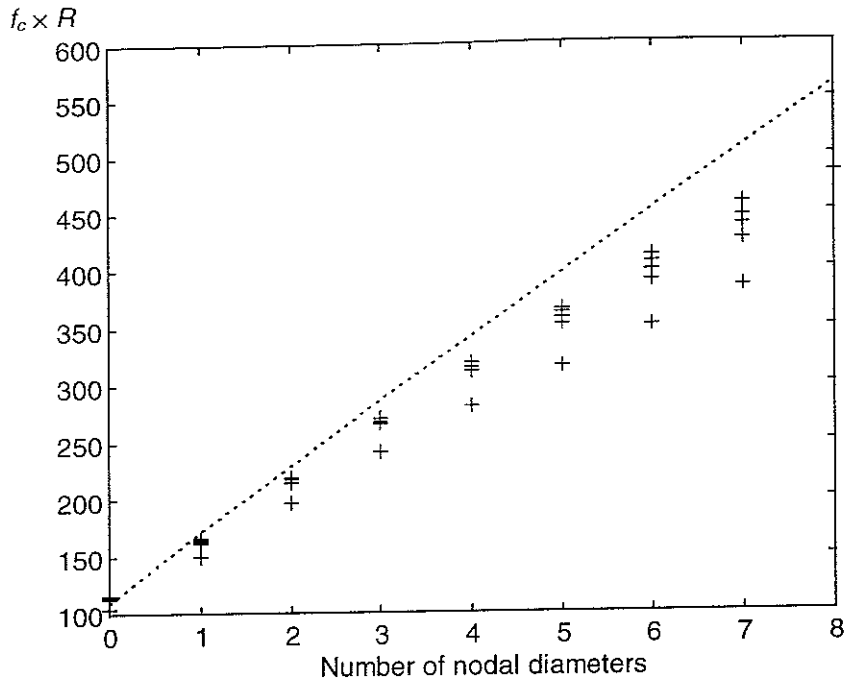

Figure 4.2. $f_c \times R$ plotted versus n, the number of nodal diameters for 0-nodal-circle modes. ····· from equation (2.3), + results from data fitting shown in Fig. 4.1.

4.3 Results for 1-nodal-circle axial modes

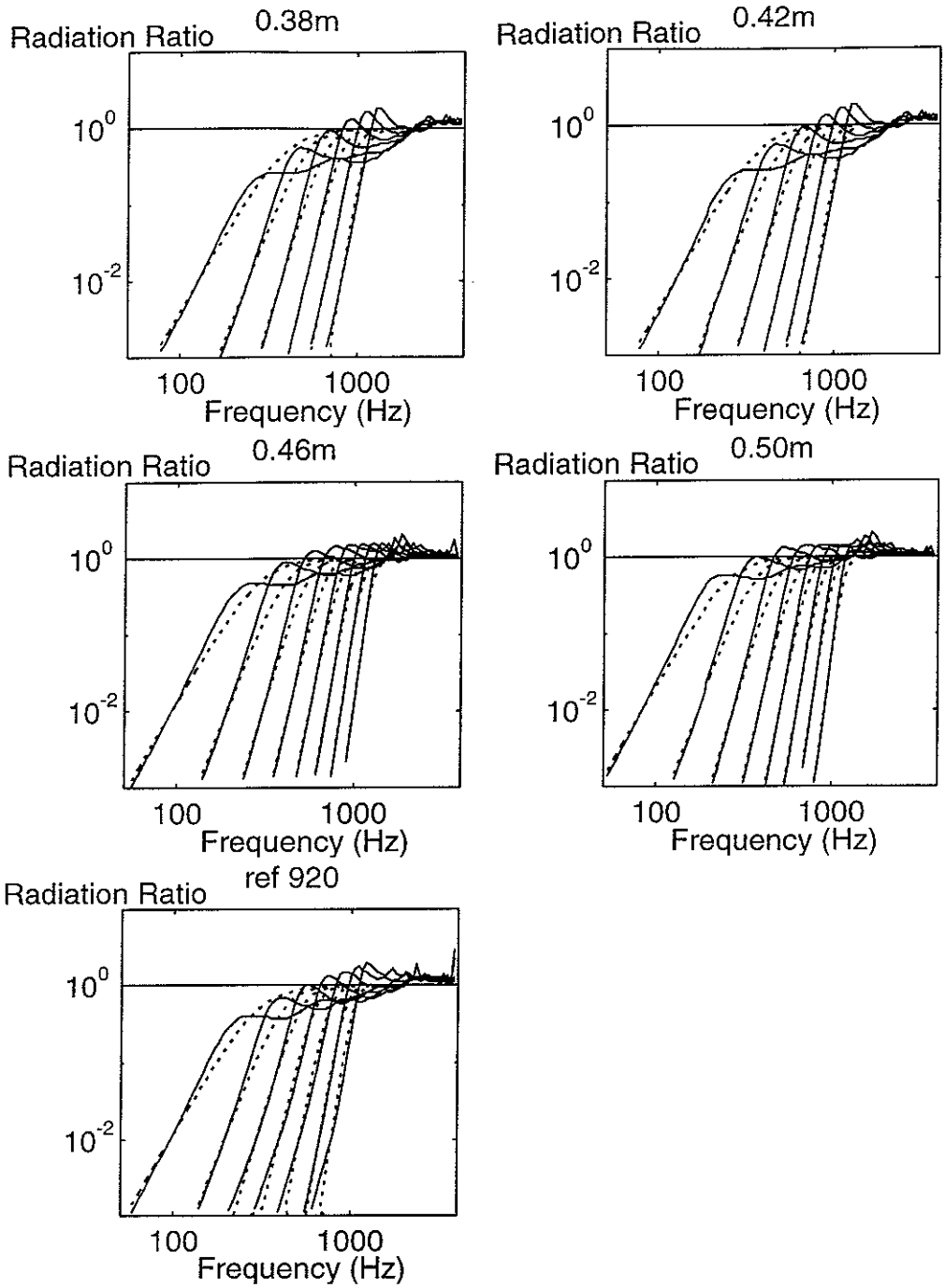

Figure 4.3. Results for 1-nodal-circle axial modes.
——, BE modelling results; - - -, approximation results.

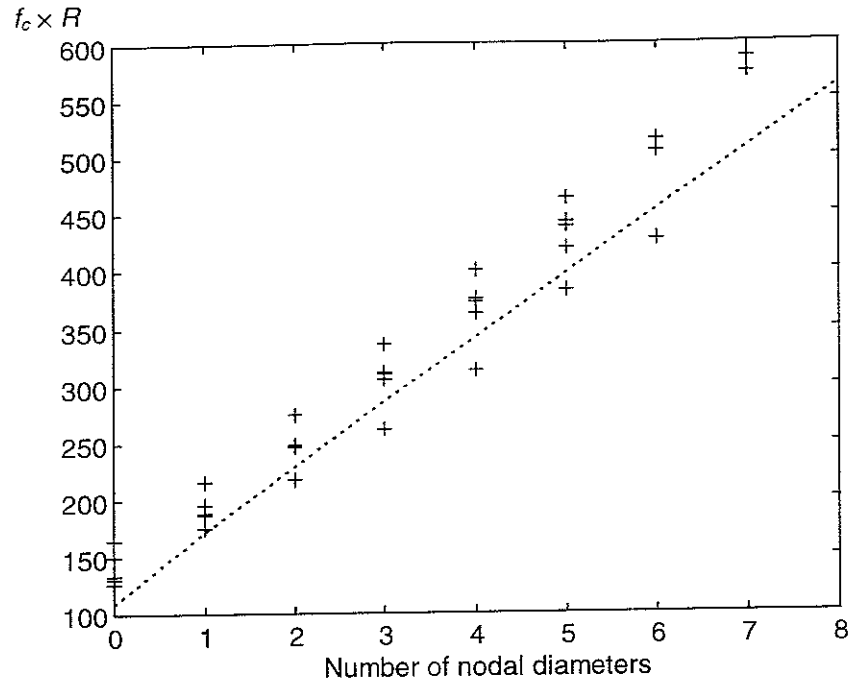

Figure 4.4. $f_c \times R$ plotted versus n, the number of nodal diameters for 1-nodal-circle modes. ..... from equation (2.3), + results from data fitting shown in Fig. 4.3.

4.4 Results for radial motion of the tyre

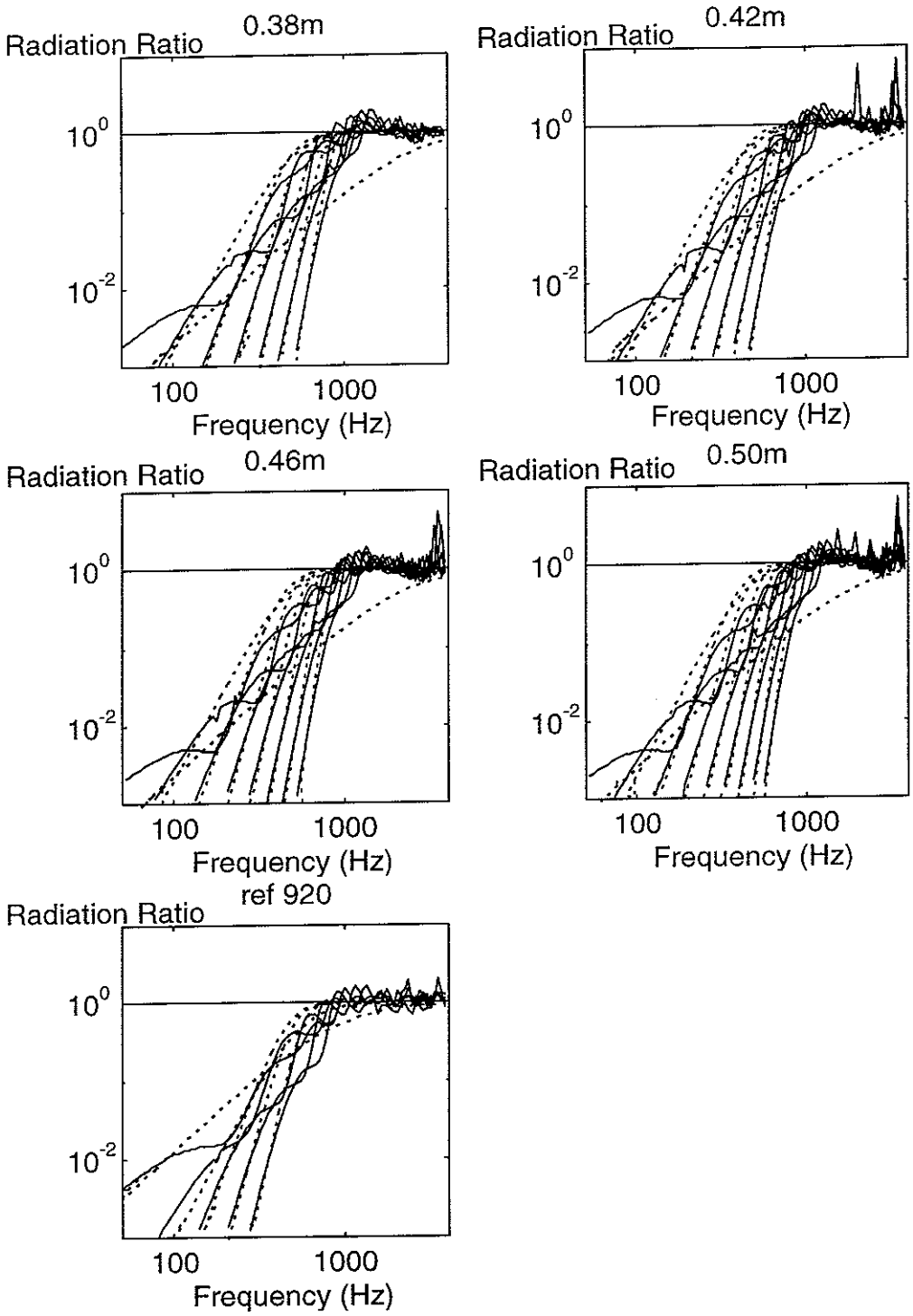

Figure 4.5. Results for radial motion with different radii.
——, BE modelling results; - - -, approximation results.

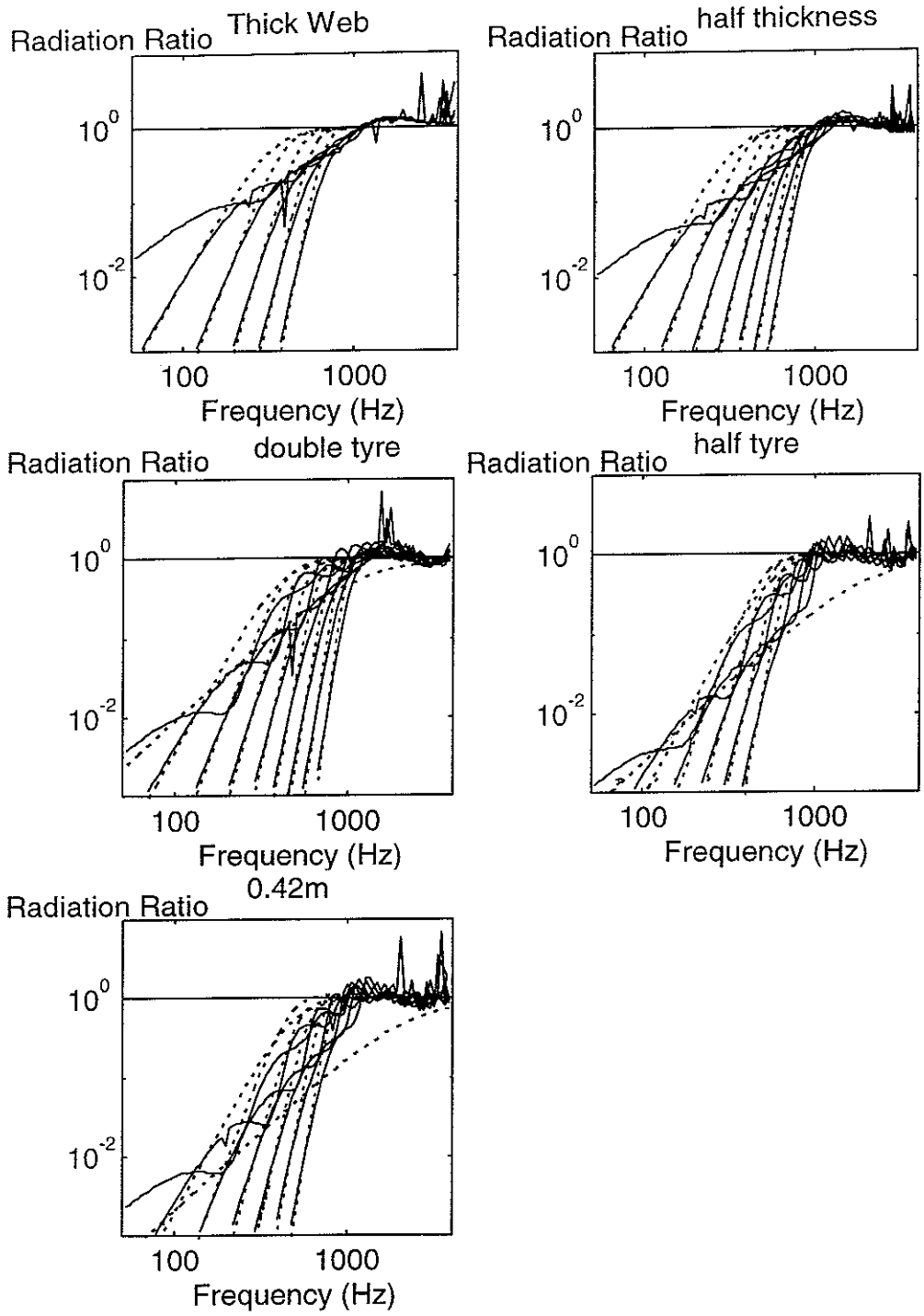

Figure 4.6. Results for radial motion with different width of web and tyre. ——, BE modelling results; - - -, approximation results.

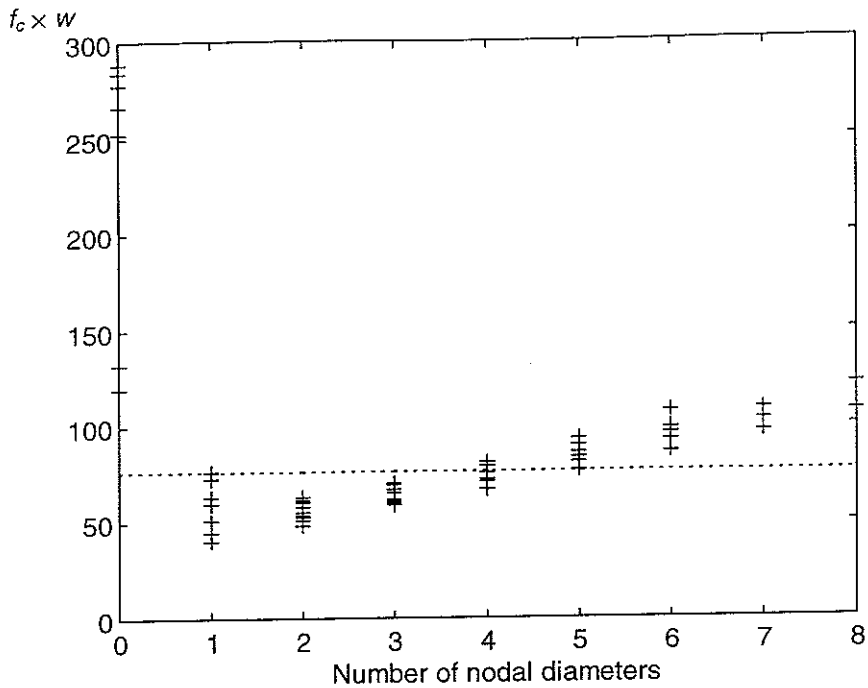

Figure 4.7. $f_c \times w$ plotted versus n, the number of nodal diameters for radial motion. ····· from equation (2.5), + results from data fitting shown in Figs. 4.5 and 4.6.

4.5 Comments

The plots presented previously show that the approximation curves provide values for the critical frequency slightly different from the ones expected with equations (2.3) and (2.5). Moreover, in the region where $\sigma < 1$ a model based on a single critical frequency does not always represent the radiation ratios sufficiently accurately, particularly for the radial motion. In the section below, the approximate formulae will be be investigated in more detail and revised formulae proposed.

5. APPROXIMATE FORMULAE

5.1 Axial motion

The radiation ratio curves for axial motion, Figures 4.1 and 4.3, have a slope f^p at low frequencies, the value of p increasing with increasing n. The curves reach $\sigma \approx 1$ at a frequency f_c which also increases with increasing n. The radiation ratio curve for a monopole has $p = 2$ and that for a dipole has $p = 4$. An axial mode with $n = 0$ resembles a dipole and thus has $p = 4$. From a consideration of the multipole nature of a mode with n nodal diameters it is found that the low frequency slope is f^p with $p = 2n+4$. This is borne out by the results in Section 4.

Figure 5.1 shows the radiation ratios of the 0-nodal-circle modes of the various wheels, plotted against $f \times r/r_0$ where f is the frequency, r is the radius and $r_0 = 0.46$. These modes are used in preferance to the 1-nodal-circle modes as the latter usually occur at frequencies above 1.5 kHz where $\sigma \approx 1$. This figure shows that the main features of the curves, in particular the frequency at which $\sigma \rightarrow 1$, are determined by the radius, r, i.e. the curves collapse togather when plotted against $f \times r/r_0$ in this manner. The dotted lines in Figure 5.1 show the result obtained by using the simple formulae given in [1] (see also Section 2):

$$\sigma_a(n) = \frac{1}{1+(f_{ca}(n)/f)^{2n+4}} \tag{5.1}$$

where

$$f_{ca}(n) = \frac{c}{2\pi r}\sqrt{(n+1)(n+4)} \tag{5.2}$$

Whilst the low frequency slopes agree with the BE predictions, the frequencies f_{ca} appear to be too high, leading to under-prediction of the radiation ratios at low frequencies.

A study has therefore been carried out in which f_{ca} has been varied in equation (5.1) using a scaling parameter μ, where

$$f_{ca}(n) = \frac{c\mu}{2\pi r} \tag{5.3}$$

The frequency range considered is limited at high frequencies to 2000 Hz, as the high frequency part of the curves is not affected by the choice of μ, and at low frequencies by the requirement $\sigma > 10^{-3}$ as smaller values do not contribute significantly to the overall noise level. The dB error in the radiation ratio has been determined at each calculation frequency within this range and for each wheel. Figure 5.2 shows this error as a function of μ. Three lines are shown for each value of n. These represent the standard deviation of the errors found at each frequency, the maximum error in the range, and the mean error in the range. Each of these quantities has also been averaged over the five wheels (the results for each wheel are similar).

In each case the three lines all show distinct minima, although these occur at different values of μ. The standard deviation has been chosen as the most robust measure of error, and the value of μ giving the minimum standard devaition has been selected for each n.

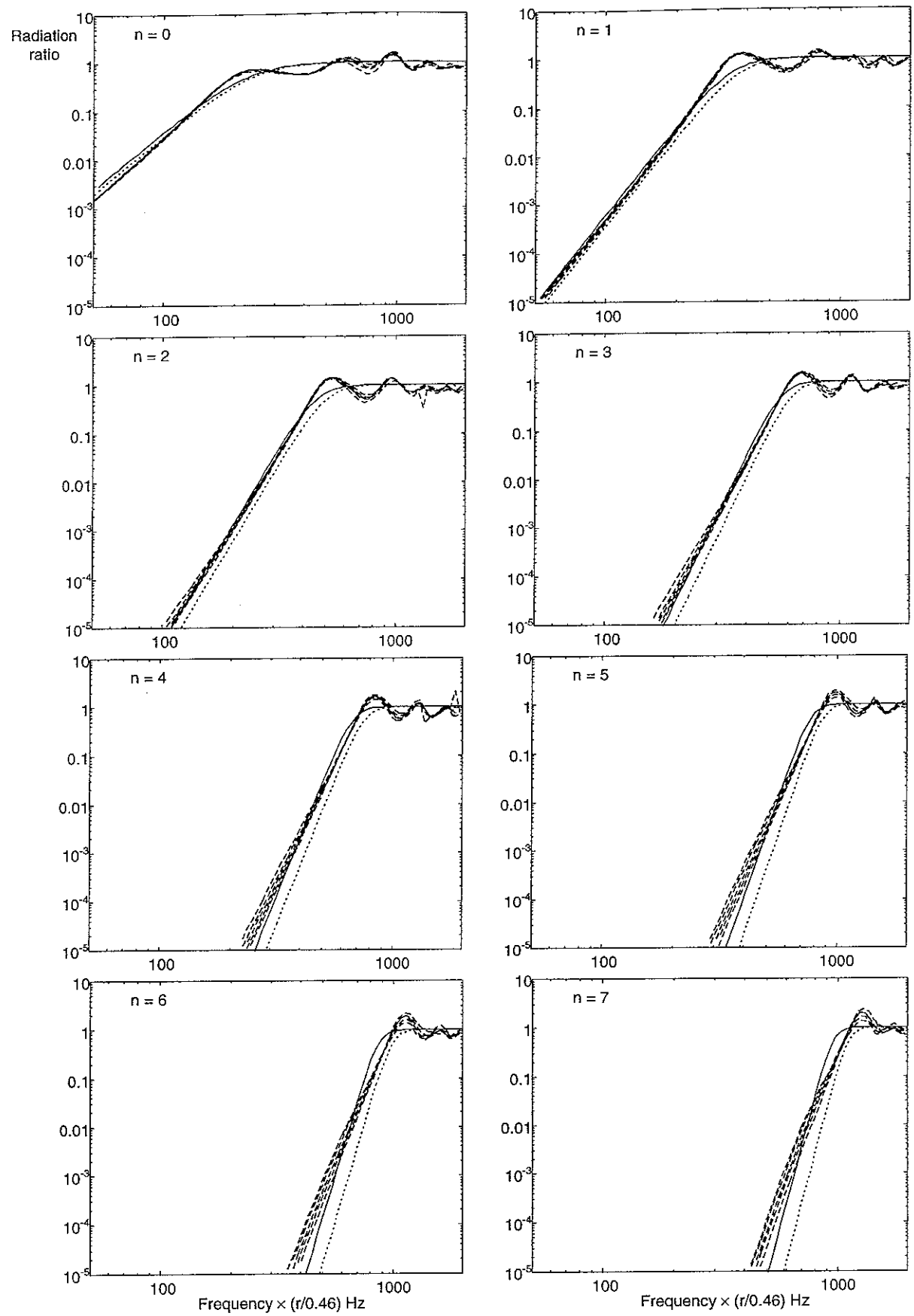

Figure 5.1 Radiation ratios of 0-nodal-circle axial modes of five wheels of different radii. – – from BE calculations, —— estimate using optimum f_c, ····· estimate using model from [1].

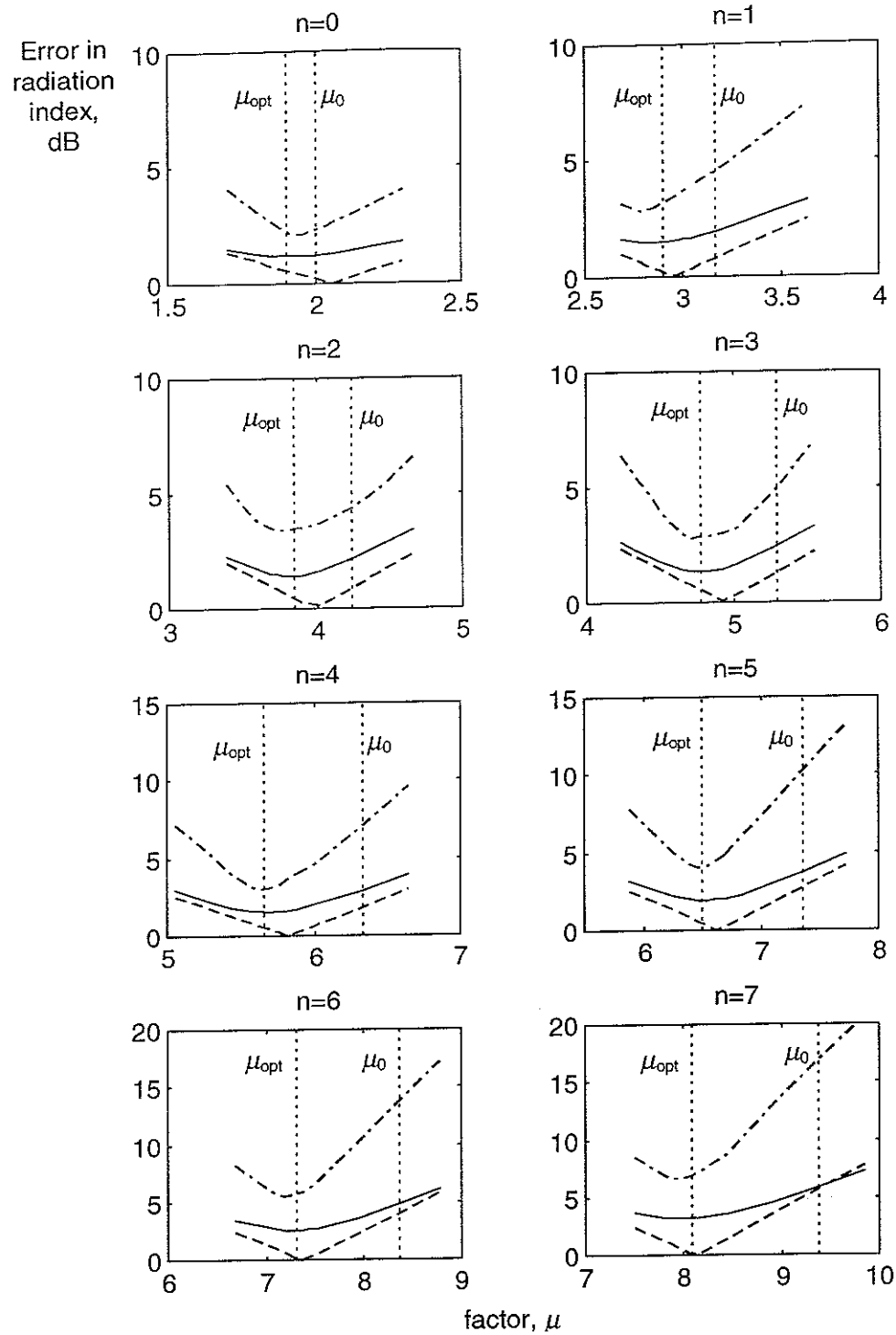

Figure 5.2 Errors in radiation index (dB) of axial 0-nodal-circle modes when using simple formula with different factors μ for determining f_c (average of five wheels). —— standard deviation of all frequency points in range, – – – mean error, – · – · maximum error, ····· optimum value of μ according to equation (5.4) and original value μ_0 according to equation (5.2).

Figure 5.3 shows this value of μ as a function of n. The function from [1] is shown as a dashed line. The dotted line is a quadratic function fitted to the values of minimum standard deviation:

$$\mu_{opt} = 1.90 + 1.015\, n - 0.0189\, n^2 \tag{5.4}$$

These values of μ are also shown by dotted lines in Figure 5.2. The radiation ratios calculated using equations (5.1, 5.3 and 5.4) are shown as solid lines in Figure 5.1.

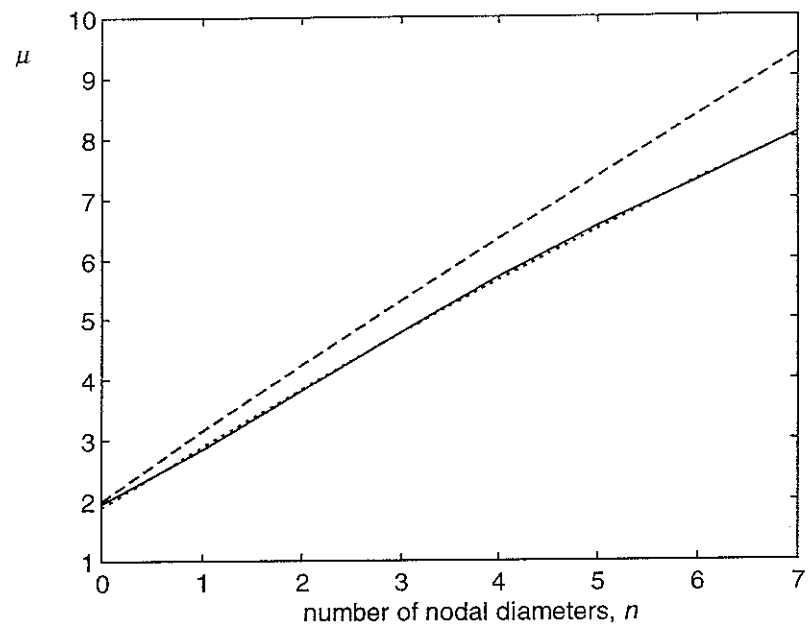

Figure 5.3 Factor μ used for determining fc for axial modes. —— from minimum standard deviation error, ····· curve fit according to equation (5.4), – – – original value μ_0 from [4] according to equation (5.2).

The errors obtained by using these formulae are shown in Figure 5.4 as a function of n. For $n \leq 4$ the standard deviation of the error is less than 1.5 dB and the maximum error is less than 3.5 dB. At higher values of n the errors increase. However, for actual wheels, modes with more than 3 nodal diameters only occur in the region well above 1 kHz where $\sigma \approx 1$, so these higher errors for larger n are not likely to lead to significant errors in predicted wheel noise.

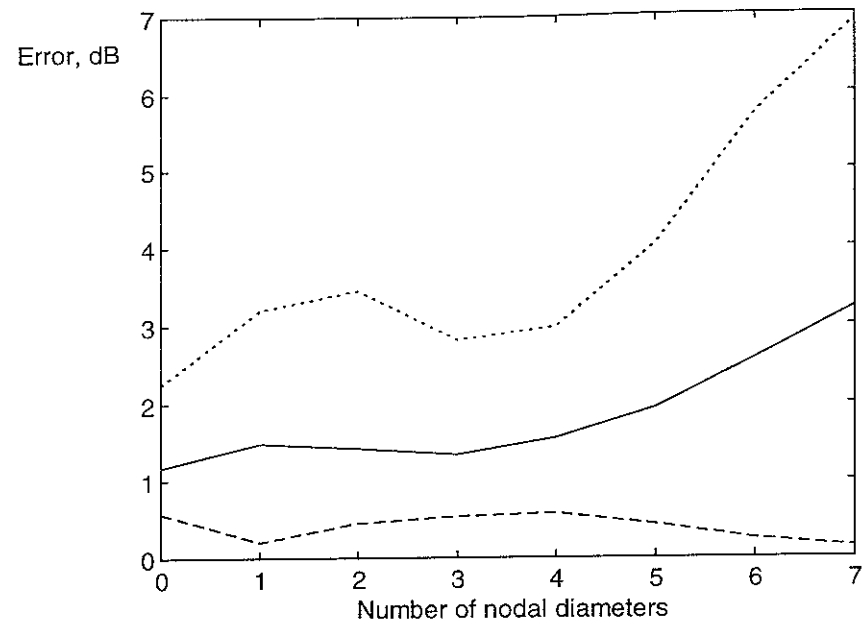

Figure 5.4 Error in radiation index (dB) of axial 0-nodal-circle modes due to the use of simple formula with optimum factors μ for determining f_c. —— standard deviation of all frequency points in range, – – – mean error, ····· maximum error.

5.2 Radial motion

5.2.1 Full web

For the radial motion, it is instructive to begin with the wheel with the full web as this has no cancellation between inner and outer tyre and therefore the curves are simpler. Figure 5.5a shows the BE predictions for $n = 0$ to 4. These results all change from $\sigma = 1$ at high frequencies to a f^2 dependence below about 1 kHz. Then a second change in gradient occurs at a lower transition frequency. Based on this structure, the proposed model is

$$\sigma_r(n) = \frac{1}{1+(f_{r2}(n)/f)^2} \quad \text{for } n = 0 \tag{5.5a}$$

$$\sigma_r(n) = \frac{1}{1+(f_{r1}(n)/f)^{2n}} \times \frac{1}{1+(f_{r2}(n)/f)^2} \quad \text{for } n > 0 \tag{5.5b}$$

where $f_{r1} = 120n$ and $f_{r2} = 800$ in this case. The results of this model are shown in Figure 5.5b.

This can be seen to give good agreement, apart from the results for $n = 0$, where the increase in σ below 200 Hz is not predicted. However, since no significant $n = 0$ radial motion occurs in practice below 1 kHz (the relevant mode of vibration occurs at about 3 kHz), this discrepancy is considered acceptable.

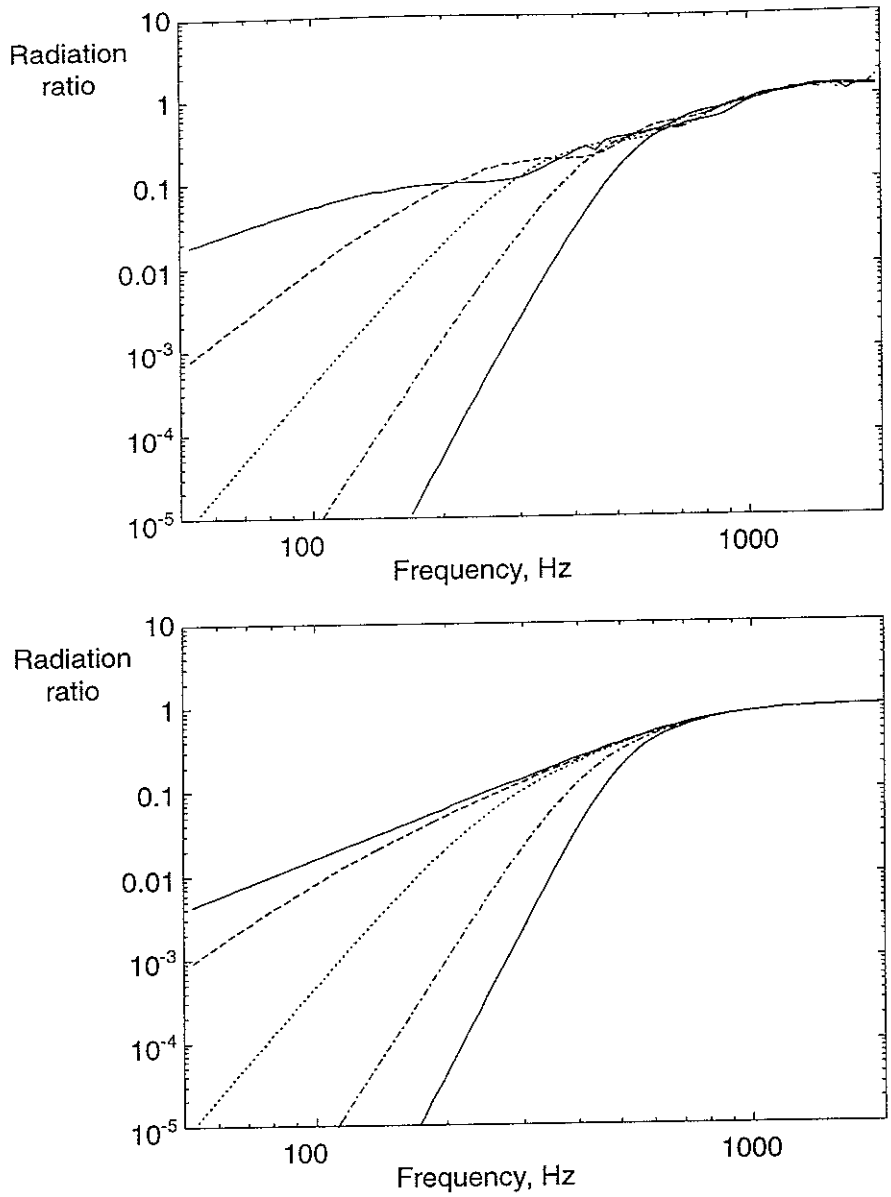

Figure 5.5 Radiation ratios for 0.42 m radius wheel with full web. —— $n = 0$, – – – $n = 1$, ····· $n = 2$, – · – · $n = 3$, —— $n = 4$ (lower line). (a) BE predictions, (b) Simple formulae (equation (5.5)).

5.2.2 Varying web and tyre dimensions

The next step is to consider the various wheels with different web and tyre dimensions. The BE predictions are shown in Figure 5.6. At high frequencies the results follow closely those for the full web (Figure 5.5) and equation (5.5) can be used to model these curves. However, at low frequencies the radiation ratio drops. It is found that the magnitude of this drop is dependent on the ratio of the areas:

$$\gamma = \frac{S_{out} - S_{in}}{S_{out} + S_{in}} \tag{5.6}$$

where S_{out} is the area of the outer surface of the tyre (the tread) and S_{in} is the area of the inner surfaces of the tyre. Thus the total area of the tyre active in radial motion is given by $S_{out} + S_{in}$.

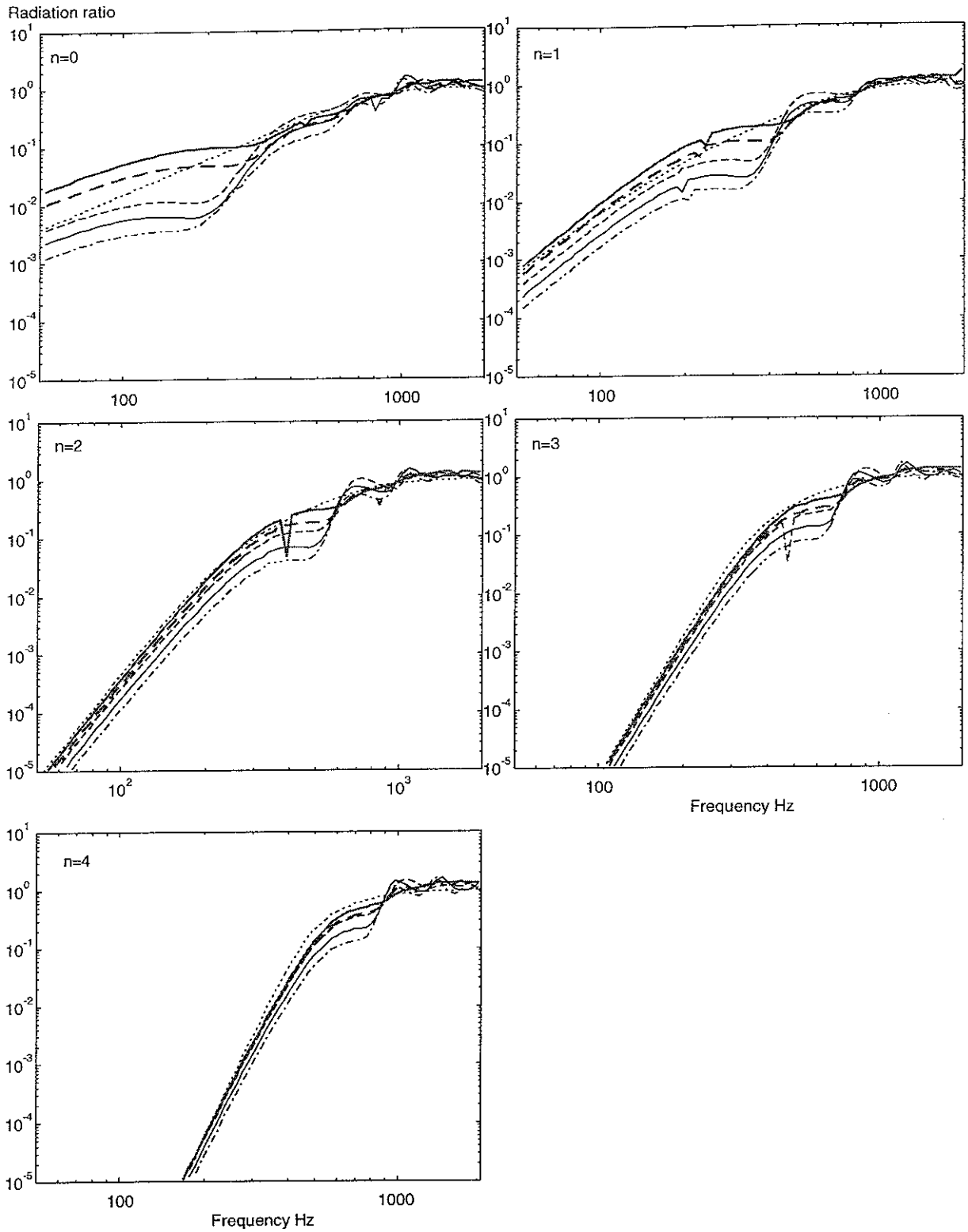

Figure 5.6 Radiation ratios predicted using BE for straight webbed 0.42 m radius wheels. —— normal wheel, – – – double thickness tyre, ····· half thickness tyre, – · – · equation (5.5), in grey: ——full web, – – – wide web.

At low frequencies, the radiation from the inner and outer surfaces tends to cancel leaving a residual area of $S_{out} - S_{in}$.

The frequency at which the radiation ratio drops is given approximately by:

$$f_{r3} = 280 + 150n \tag{5.7}$$

For frequencies below f_{r3} it is found that the radiation ratio is reduced from that given by equation (5.5) by a factor of approximately $\sqrt{\gamma}$. The resulting predictions are given in Figure 5.7 which may be compared with the BE results of Figure 5.6. Using this factor works well for $n \geq 2$. For $n = 0$ the factor should be nearer to γ but, as noted above, the prediction for the full webbed wheel is less accurate anyway at $n = 0$, and in any case the results are unlikely to be significant as $n = 0$ radial motion does not occur at low frequencies.

5.2.3 Varying radii

The final stage is to consider the effect of wheel radius, r. Whereas the radiation from axial motion depended directly on $1/r$, for the radial motion the various transition frequencies, f_{r1}, f_{r2} and f_{r3} are found to depend on $1/\sqrt{r}$. The BE results for various radii are shown in Figure 5.8 plotted against frequency factored by $\sqrt{(r/0.46)}$. Good agreement can be seen.

5.2.4 Summary

To summarise, the following formulae are used for the radial motion:

$$\sigma_r(n) = \frac{\Gamma}{1 + (f_{r2}(n)/f)^2} \qquad \text{for } n = 0 \tag{5.8a}$$

$$\sigma_r(n) = \frac{\Gamma}{1 + (f_{r1}(n)/f)^{2n}} \times \frac{1}{1 + (f_{r2}(n)/f)^2} \qquad \text{for } n > 0 \tag{5.8b}$$

where

$$\Gamma = \sqrt{\frac{S_{out} - S_{in}}{S_{out} + S_{in}}} \qquad \text{for } f < f_{r3} \tag{5.9a}$$

$$\Gamma = 1 \qquad \text{for } f > f_{r3} \tag{5.9b}$$

and

$$f_{r1} = 120n / \sqrt{(r/0.42)} \tag{5.10a}$$

$$f_{r2} = 800 / \sqrt{(r/0.42)} \tag{5.10b}$$

$$f_{r3} = (280 + 150n) / \sqrt{(r/0.42)} \tag{5.10c}$$

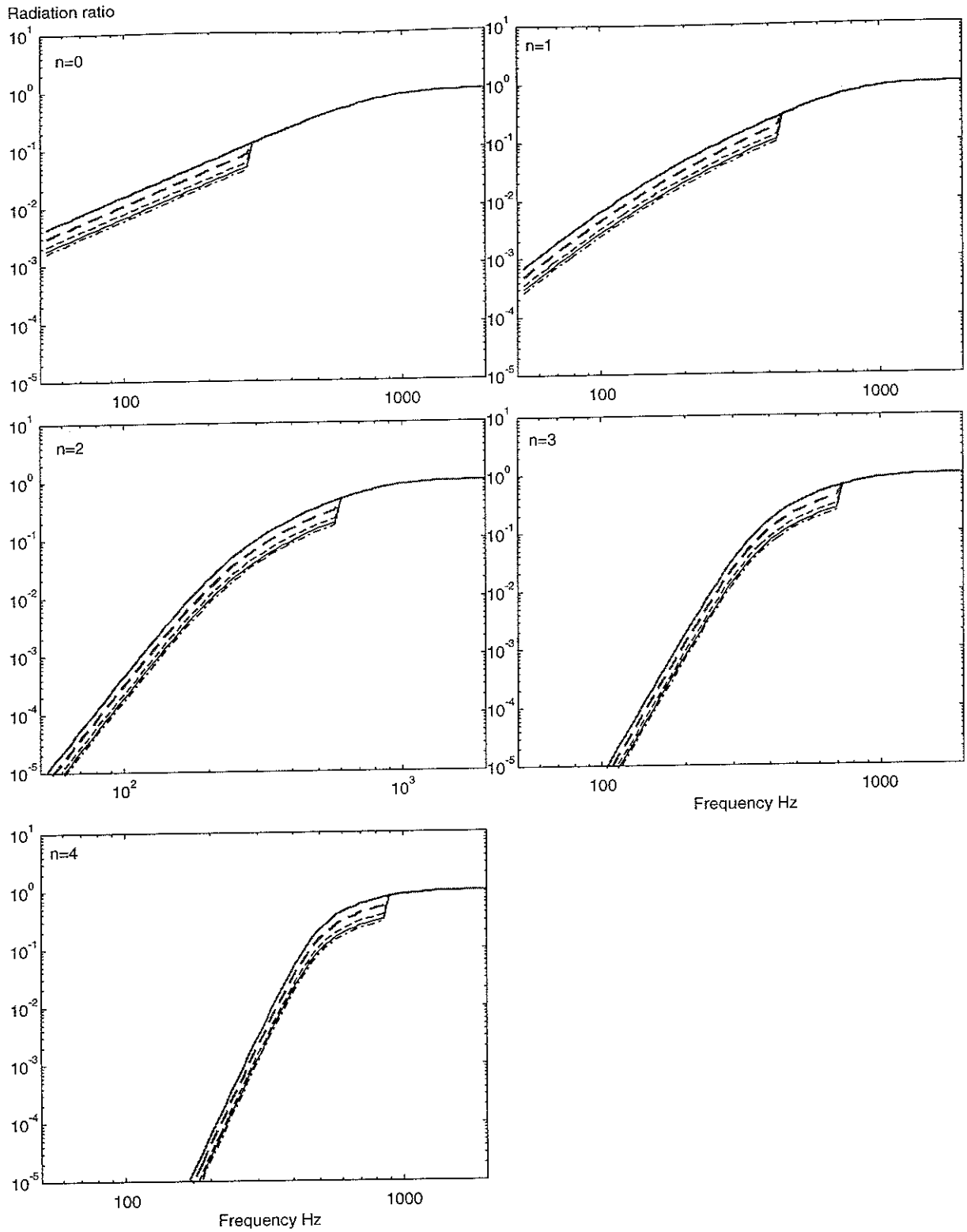

Figure 5.7 Radiation ratios predicted using simple formulae for straight webbed 0.42 m radius wheels. —— normal wheel, – – – double thickness tyre, ····· half thickness tyre, in grey: —— full web, – – – wide web.

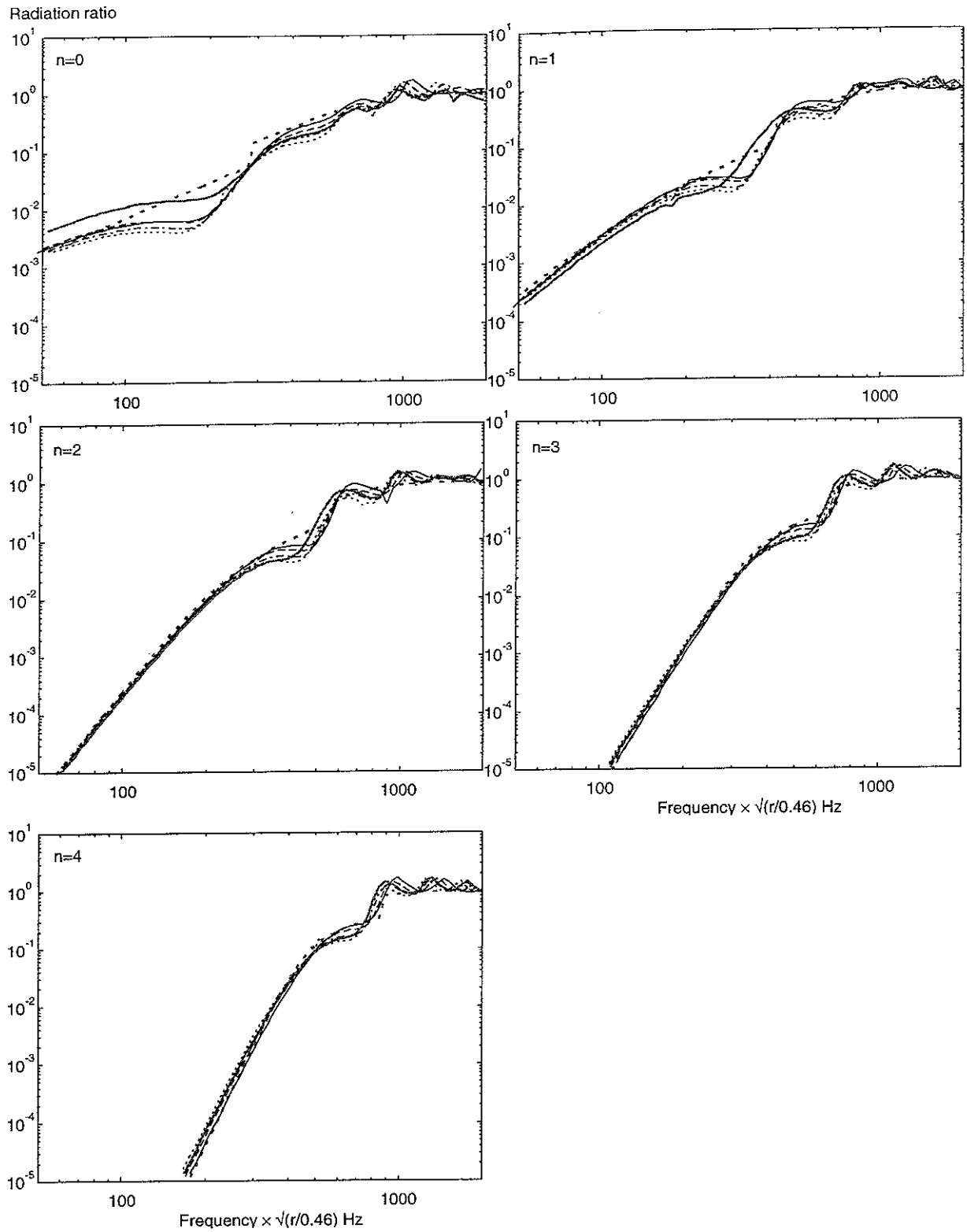

Figure 5.8 Radiation ratios predicted using BE for straight webbed wheels of different radii. —— 0.38 m, – – – 0.42 m, – · – · 0.46 m, ····· 0.50 m, in grey: —— reference freight wheel (0.46 m radius), ····· simple formulae.

5.3 Effect on TWINS predictions

In this report, the simple formulae used within the TWINS program for the radiation ratios of wheels have been shown to be inadequate and improved formulae have been proposed. In this section the effect of changing TWINS to include the new formulae is evaluated. Results are presented only for the 920 mm standard freight wheel (Figure 3.1). These are given in Figure 5.9 in which the total wheel noise and the components due to axial and radial motion are shown separately. The predictions marked 'new' are based on the formulae developed in this section of the report, whilst those marked 'previous' are based on the formulae listed in Section 2 (as revised in ref. [4]). The predictions marked 'old' are based on the formulae in ref. [1] prior to ref. [4].

It can be seen that although the low frequency results are affected especially for the radial component, the results in the region above 500 Hz, which usually dominate the A-weighted level, are hardly affected at all. This is confirmed by the fact that the A-weighted level is only modified by –0.3 dB compared to the 'previous' version and +0.6 dB compared to the 'old' version. These changes are due to the radial component, the axial component being hardly affected at all.

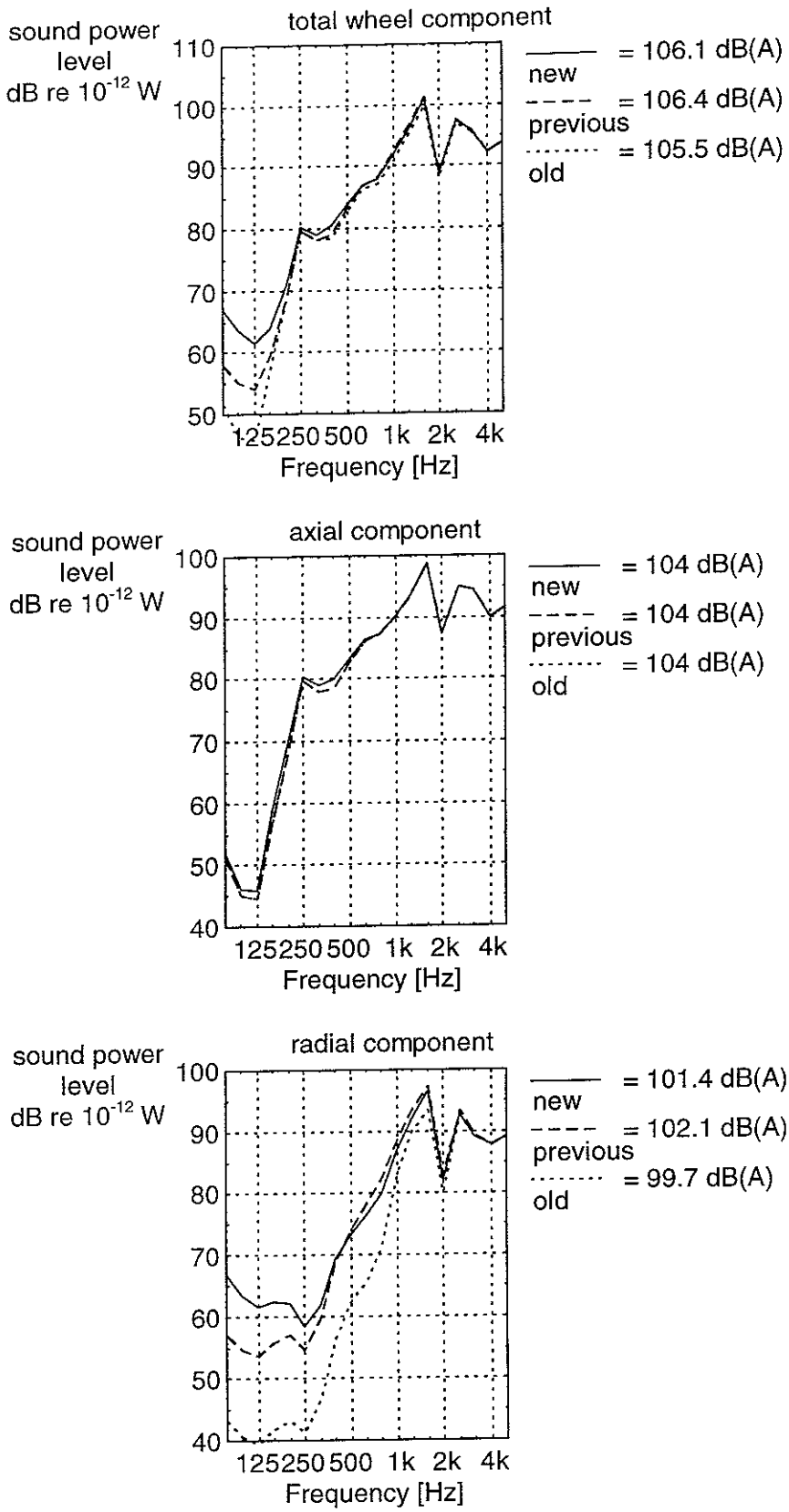

Figure 5.9 Sound power component radiated by the wheel predicted using different versions of TWINS for 920 mm diameter freight wheel.

6. CONCLUSIONS

The Sysnoise software has been used to perform BE calculations of the sound radiation from wheels using the axi-harmonic formulation. Results in terms of radiation ratios for the various mode shapes have been compared with semi-analytical formulae as implemented in TWINS. As a result of this more rigorous study, revised formulae have been devised which give better agreement with the BE results. These new formulae have been implemented in the TWINS wheel radiation module. For the 920 mm reference freight wheel, the results are not affected significantly, although the low frequency radial component is increased. However, the new formulae should be more robust for studying different wheel geometries. Nevertheless, for radically different wheel designs it is recommended that specific BE calculations be performed to complement the TWINS predictions.

7. REFERENCES

1. D.J. Thompson, M.H.A. Janssens, TWINS: Track-Wheel Interaction Noise Software. Theoretical manual, version 2.4, TNO report TPD-HAG-RPT-93-0214, revised Jan 1997.

2. D.J. Thompson, Railway rolling noise - a study of models for the sound radiation from wheels, TNO report TPD-HAG-RPT-91-0181, November 1991.

3. N.S. Ferguson, Sound power calculations for railway wheels using the boundary element method, ISVR Contract Report No. 97/02, January 1997 (Silent Freight project confidential).

4. D.J. Thompson, N.S. Ferguson, C.J.C. Jones, Silent Freight Task 3.1.2. Modelling the sound power radiated by a wheel. ISVR Contract Report 97/28, August 1997 (project confidential).

5. SYSNOISE manual, version 5.3. LMS International.

6. ANSYS manual, version 5.4.

APPENDIX A - DETAILS OF A RAILWAY WHEEL

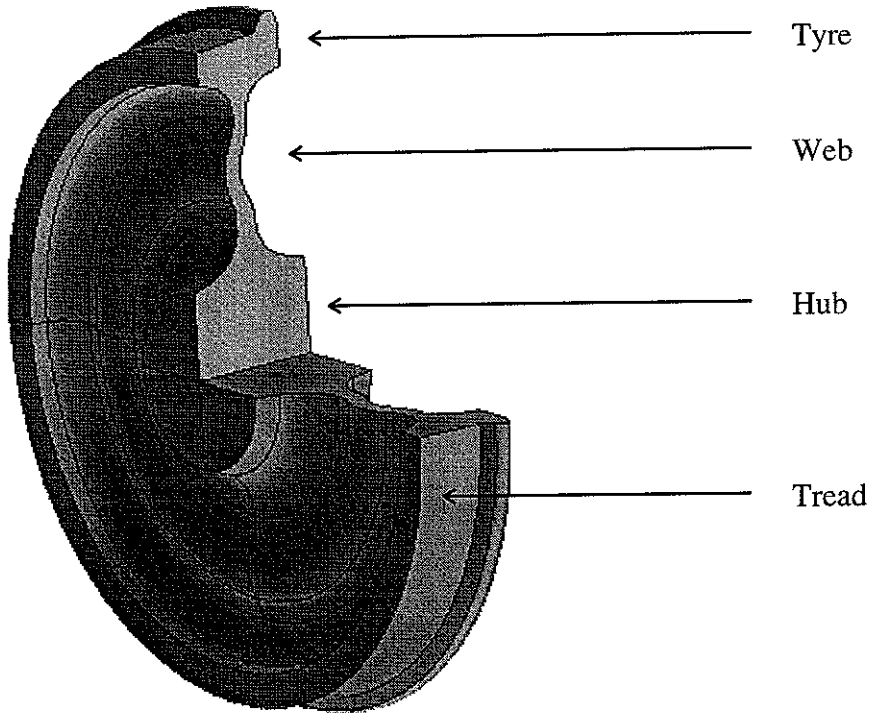

APPENDIX B: THE FINITE ELEMENT METHOD FOR MODAL ANALYSIS OF AXISYMMETRIC ELASTIC STRUCTURES

The finite element method is a general method for solving a wide range of problems. Here the finite element equations for the dynamics of linear elastic bodies is briefly described (based on ref [A1]).

The procedure of this method is:

1. Divide the structure up into a number of elements of finite size. (the elements are assumed to be joined together at node points.)

2. Associate with each node point a given number of degrees of freedom.

3. Construct a set of functions for an element such that each one gives a unit value for one degree of freedom and zero values for all the others.

4. Substitute the assumed functions for an element into the expressions for:
   (i) kinetic energy,
   (ii) strain energy,
   (iii) virtual work done by the applied forces in a virtual displacement,
to give expressions in terms of nodal degrees of freedom.

5. Add the energies for each element together to give energies for the complete structure.

6. Use the energy expressions to derive the equations of motion of the complete structure in terms of the nodal degrees of freedom (Lagrange's equations).

The governing equation used in the finite element method is derived here by using the Lagrangian functional and its associated differential equation. The Lagrangian is defined as follows:

L = kinetic energy - potential energy

The potential energy of the system is the sum of the strain energy and the work done by external forces acting on the structure. We integrate the strain energy density over the volume of the structure and the work done by the loads is simply calculated as force times displacement. The total kinetic energy is found by integrating the kinetic energy of each volume element of the structure. Hence, if $\underline{U}_p$ represents the displacement of a point P, $\underline{F}$ the externally applied forces represented as a distributed force per unit volume, and $\underline{\varepsilon}$, $\underline{\sigma}$ the strain and stress respectively at that point, then

$$\text{Potential Energy} = \int_V [\frac{1}{2}\varepsilon^T.\sigma + \underline{F}^T \underline{U}_P]dV \qquad \text{(A1)}$$

$$\text{Kinetic Energy} = \int_V \frac{1}{2}\rho \dot{\underline{U}}_P{}^T \dot{\underline{U}}_P \, dV \qquad \text{where } \rho \text{ is the density.} \qquad \text{(A2)}$$

Now using the expression for strain, $\underline{\varepsilon} = G.\underline{U}_P$, in which G is a matrix representation of the gradient operator, and the stress-strain relation, $\underline{\sigma} = D\underline{\varepsilon}$, the matrix D being calculated from the modulus of elasticity, the finite element method interpolating the displacement can be applied.

On each element $\underline{U}_P = N\underline{U}^e$ where N is a matrix of 'shape functions' and $\underline{U}^e$ is a vector of the unknown displacement at each node.

The volume integral becomes the sum of the integrals over each element. Hence,

$$L = \sum_e \left\{ \int_{V^e} \left[\frac{\rho}{2} \dot{\underline{U}}^{eT} N^T N \dot{\underline{U}}^e - \frac{1}{2} \underline{U}^{eT} N^T G^T DGN \underline{U}^e \right] dV^e + \underline{F}^{eT} \underline{U}^e \right\} \tag{B3}$$

The Lagrangian equation [A1] is

$$\frac{\partial L}{\partial \underline{U}} = \frac{d}{dt}\left(\frac{\partial L}{\partial \dot{\underline{U}}} \right) + \sum_e \underline{C}^e \dot{\underline{U}}^e \tag{B4}$$

Where $\underline{U}$ is the vector of all nodal values and $\sum_e \underline{C}^e \dot{\underline{U}}^e$ is added to take account of the non-conservative forces. These forces are modelled here as equivalent viscous damping.

The Lagrangian equation becomes

$$\sum_e \left[M^e \ddot{\underline{U}}^e + C^e \dot{\underline{U}}^e + K^e \underline{U}^e - \underline{F}^e \right] = 0 \tag{B5}$$

where

$$K^e = \int_{V^e} N^T G^T DGN.dV^e \text{ and } M^e = \int_{V^e} N^T.\rho.N.dV^e \tag{B6}$$

Globally, the equation becomes

$$M\ddot{\underline{U}} + C\dot{\underline{U}} + K\underline{U} = \underline{F} \tag{B7}$$

where $\underline{U}$ is the vector representing the displacements in each degree of freedom in the global system.

The structure that has been dealt with is axisymmetric and axi-harmonic solutions for displacement are sought *i.e.* solutions in which the displacements are specified to vary with the circumferential angle as cos nθ. The element matrices then become:

$$K^e = \int_{element} N^T G^T DGNr\cos n\theta.drdzd\theta \text{ and } \quad M^e = \int_{element} N^T.\rho.N.r\cos n\theta.drdzd\theta \tag{B8}$$

The final step in deriving the system equation to be used here is to make the assumption that the time variation in the applied forces is sinusoidal, *i.e.*,

$$\underline{F} = \underline{f}e^{j\omega t} \tag{B9}$$

The resulting displacements will then also be sinusoidal,

$$\underline{U} = \underline{u}e^{j\omega t} \tag{B10}$$

The system equation which is used becomes

$$(-\mathbf{M}\omega^2 + j\mathbf{C}\omega + \mathbf{K})\underline{u} = \underline{f} \tag{B11}$$

In order to find the natural frequencies of the structure and the corresponding mode shapes, the damping in the system is neglected and the matrix equation of motion is solved as an eigenvalue problem without forcing.

$$(-\omega^2\mathbf{M} + \mathbf{K})\underline{a} = \underline{0} \tag{B12}$$

or

$$\mathbf{M}^{-1}\mathbf{K}\,\underline{a} = \omega^2\,\underline{a} \tag{B13}$$

The eigensolution of the square matrix $\mathbf{M}^{-1}\mathbf{K}$ yields the natural frequencies ω_n and the corresponding eigenvectors of displacement $\underline{a}_n$ represent the mode shapes of the structure. Since the number of nodal diameters is specified in the formulation the modal solution must be carried out for each possible axi-harmonic number n in order to produce all the possible modes of the structure.

Reference

[A1] M Petyt 'Introduction to finite element vibration analysis' Cambridge University Press, 1990.

APPENDIX C - THE BOUNDARY ELEMENT METHOD FOR PREDICTION OF THE RADIATION RATIO.

Whereas the finite element method is a general method for solving differential equations on arbitrarily shaped domains, the Boundary Element Method (BEM) is based on a boundary integral equation representation of the problem. For the calculation of acoustic wave fields the differential equation to be solved is the reduced Kirckhoff-Helmholtz form of the wave equation:

$$(\nabla^2 + k^2)\, p(x) = -Q(x) \qquad \text{(B1)}$$

where k is the wave number (ω/c), and $p(x)$ is the pressure at point x in the domain. $Q(x)$ represents the acoustic source strength distribution.

The corresponding integral equation which can be derived from the equation above is [B1]:

$$\int_S [g(x,y)\nabla_y p(y) - p(y)\nabla_y g(x,y)].ndS = \varepsilon p(x) \qquad \text{(B2)}$$

where g(x,y) is the solution for a unit point source and is called the Green's function. In three dimensions

$$g(x,y) = \frac{e^{-jkr}}{4\pi r}, \quad r = |x-y| \qquad \text{(B3)}$$

The derivative of pressure normal to the surface S is closely associated with the particle velocity, since $\underline{n}.\nabla_y p(y) = \dfrac{\partial p}{\partial \underline{n}} = -j\omega\rho_0 v_n$. The formulation therefore describes the acoustic field at a point x away from the surface S in terms of the normal velocity and pressure at all points y' on the boundary, S, of the domain.

If the point x is allowed to become a surface point itself, y', then the boundary integral equation is obtained;

$$\int_S [g(y',y)\nabla_y p(y) - p(y)\nabla_y g(y',y)].ndS = \varepsilon.p(y') \qquad \text{(B4)}$$

where for a smooth surface the term $\varepsilon = 1/2$. Equation (B4) links the pressure at a single point of the surface to the pressure and normal velocities at all points on the surface.

The formulation is now discretized using the finite element approximation method. Introducing shape functions within each element assume

$$p = [N_a]\{p\}_e \text{ and } \quad \frac{\partial p}{\partial n} = [N_s]_e \left\{\frac{\partial p}{\partial n}\right\}_e \qquad \text{(B5)}$$

Substitute into the surface integral equation and evaluate for the point y' being at node i. This gives

$$p_i = \sum_e [m]_e \left\{\frac{\partial p}{\partial n}\right\}_e - \sum_e [d]_e \{p\}_e \qquad \text{(B6)}$$

Where

$$[m]_e = 2\int_{S_e} g(y_i, y)[N_s]_e \, dS \quad \text{and} \quad [d]_e = 2\int_{S_e} \frac{\partial g}{\partial n}(\underline{y_i}, \underline{y})[N_a] dS \qquad \text{(B7)}$$

Combining equations for all nodes $\underline{i}$ produces a square set of equations.

$$\{p\} = [M]\left\{\frac{\partial p}{\partial n}\right\} - [D]\{p\} \qquad \text{(B8)}$$

Where {p} and {∂p/∂n} are vectors of nodal values for the whole surface. If the normal velocity is specified on nodes of the surface, Equation (B8) represents a set of equations with the values $\{p\}$ as unknowns. It may therefore be solved for the pressures at all nodes on the surface.

Now that the pressure and velocity are known, the acoustic intensity on the surface is calculated as

$$I = \text{Re}\ \{p^*(y)\, v_n(y)\} \qquad \text{(B9)}$$

and this can be integrated over the surface to give the total radiated sound power

$$W = \int_S I.n \, dS \qquad \text{(B10)}$$

and the radiation ratio calculated as

$$\sigma = \frac{W}{\left\langle \overline{v^2} \right\rangle S \rho c} \qquad \text{(B11)}$$

where $\left\langle \overline{v^2} \right\rangle$ is the space averaged mean square normal velocity (evaluated as the squared velocity integrated over the surface) and ρc is the specific impedance of air.

The software package SYSNOISE [B2] implements a number of variations to the basic BEM. For the calculations of the present work a formulation of the problem called the 'indirect formulation', was chosen. The reasons for this choice are that:

1. in SYSNOISE a method is used with this formulation that avoids some mathematical problems for external radiation problems
2. only with the indirect BEM does SYSNOISE implement a solution for axisymmetric structures where the specified normal velocity distributed over the surface of the body is decomposed in term of a Fourier series of components in θ. This allows a direct method of calculating the radiation ratios of the structural modes of the wheel, having n nodal diameters.

References

[B1] Fundamentals of Noise and Vibration, F Fahy and J Walker, (Eds), E & FN Spon, London, 1998.

[B2] SYSNOISE Revision 5.0 Theoretical manual, Numerical Integration Technologies, First Edition, 1993.

APPENDIX D - SYSNOISE JOURNAL FILE LISTING OF THE MODELLING OF A WHEEL RADIATION.

Example of the radial motion, 2-nodal-diameter for the wheel radius 0.38m.

```
New Name 'MODEL2' Model 2 File model2.sdb Return
Option  BEM  Indirect  Variational  Node  Exterior  Uncoupled  Unbaffled  NoAsymptotic
Frequen Return
Input Mesh Format Ansys File "t38bem.cdb" Return
TwoDimensional Return


;       Reverse elements for the consistency of the normal vectors.
Reverse
   Element 12 to 20, 80 to 90, 69 to 71, 113 to 121
   Return

;       Definition of the set of elements where the boundary conditions are to be applied.
Set 1          ; Part of surface inside the axle where velocity is to be zero.
   Elements 104 to 121
   Return
Set 2
   Elements all
   Return
Set 3 Difference 2 1 Return          ; Part corresponding to surface of ANSYS model,
                                     ; 't38.cdb'.

;       Generation of the boundary conditions (stored in the 'rad38d2.rst' file and defined on
;       the mesh 't38.cdb').
Generate
   Element set 3
   From Displacements File  "rad38d2.rst" Format Ansys
   Load 1
   Mesh File  "t38.cdb" Format Ansys
   Algorithm  1  Tolerance 0.049037 Average 4
   Return

;       Definition of the axisymmetry allowing the calculations for a 2-nodal-diameter case.
AxiSymmetry Refinement 2  Harmonic 2 Return

;       Definition of the field point mesh.
Point Sphere 0 0 0 Radius 0.6 Divide 60 Return

;       Calculation along the frequency range defined of the harmonic chosen.
Response
   Frequency 50 To 6000 LogStep 1.05
   Harmonic 2              ; Selector of harmonic terms to be used.
   Save Potentials Step 1
```

```
   Save Displacements Step 1
   Save Results Step 1
   Near 2
   Far 5
   Quadrature 2 2 1
   Return

;        Stores the results in 'Power.res'.
Extract Power Return
```

APPENDIX E - DATA TREATMENT. M-FILE PLOTTING THE RESULTS AND GIVING THE CRITICAL FREQUENCY AS AN OUTPUT.

Example of the 0-nodal-circle results for the wheel radius 0.38m.

```
function out=calc31(s0)

figure
A=[1];

for j=0:5
i=1;
name1=['t381' int2str(j) '.m'];
fi1=fopen(name1,'r');
A1=fscanf(fi1,'%f');
a1=length(A1);
f1=A1(1:3:a1,1);
sigmafp1=A1(2:3:a1,1);
sigma1=A1(3:3:a1,1);
%
%       Omits discontinuities.
%
k=find(sigmafp1(:,1)>2);
sigmafp1(k,1)=NaN*ones(size(k));
%
%       Plots the radiation ratio.
%
subplot(2,1,1)
loglog(f1,sigmafp1,'g')
hold on
%
%       Calculation of fc with an interpolation.
%
while ((sigmafp1(i,1)<s0)&(i<99))
        i=i+1;
end

if ((sigmafp1(i,1)>s0)&(i>1))
        t=((s0-sigmafp1(i,1))/(sigmafp1(i-1,1)-sigmafp1(i,1)));
        f0=t*f1(i-1,1)+(1-t)*f1(i,1);
        fc=f0*(1/s0-1)^(1/(2*j+4));

else
        fc=NaN;
end
%
%       Plots the approximation of the radiation ratio.
%
```

```
sigapp=1./(1+(f1.\fc).^(2*j+4));
loglog(f1,sigapp,'m:')

%
%       Stores the critical frequency in the matrix A.
%
A(j+1,:)=[fc];


end


ylabel('radiation efficiency')
xlabel('frequency (Hz)')
title('0.38m 1-nodal-circle')
hold on
axis([50 6000 1e-5 10])
grid off
x=[50 6000];
y=[1 1];
loglog(x,y,'y')

legend('g-','modelling results','m:','approximation',-1)

%
%       Plot of fc Vs the number of nodal diameters.
%
r=0.38;
n=[0:1:length(A)-1];
subplot(2,1,2)
plot(n,A*r,'go')
hold on
plot(n,(fR(n)),'m:')
ylabel('fc * R')
xlabel('number of nodal diameters')
title('fc.R Vs n')
legend('go','modelling results','m:','approximation',-1)
%
%       Gives the list of critical frequencies as an output.
%
out=A;


fclose('all');
```